REPORT 1328

A SECOND-ORDER SHOCK-EXPANSION METHOD APPLICABLE TO BODIES OF REVOLUTION NEAR ZERO LIFT[1]

By CLARENCE A. SYVERTSON and DAVID H. DENNIS

SUMMARY

A second-order shock-expansion method applicable to bodies of revolution near zero lift is developed. Expressions defining the pressures on noninclined bodies are derived by the use of characteristics theory in combination with properties of the flow predicted by the generalized shock-expansion method. This result is extended to inclined bodies to obtain expressions for the normal-force and pitching-moment derivatives at zero angle of attack. The method is intended for application under conditions between the ranges of applicability of the second-order potential theory and the generalized shock-expansion method— namely, when the ratio of free-stream Mach number to nose fineness ratio is in the neighborhood of 1.

For noninclined bodies, the pressure distributions predicted by the second-order shock-expansion method are compared with existing experimental results and with predictions of other theories. For inclined bodies, the normal-force derivatives and locations of the center of pressure at zero angle of attack predicted by the method are compared with experimental results for Mach numbers from 3.00 to 6.28. Fineness ratio 7, 5, and 3 cones and tangent ogives were tested alone and with cylindrical afterbodies up to 10 diameters long. In general, the predictions of the present method are found to be in good agreement with the experimental results. For noninclined bodies, pressure distributions predicted with the method are in good agreement with existing experimental results and with distributions obtained with the method of characteristics. For inclined bodies, the normal-force derivatives per radian (for normal-force coefficients referenced to body base area) are predicted within ±0.2 and the locations of the center of pressure are predicted within ±0.2 body diameters. On the basis of these results, the second-order shock-expansion method appears applicable for values of the ratio of free-stream Mach number to nose fineness ratio from 0.4 to 2.

INTRODUCTION

The flow about bodies traveling at high supersonic speeds was investigated by Eggers and Savin (ref. 1). They found that under specified conditions such flows could be considered as locally two-dimensional and could be treated by a generalized shock-expansion method. This method has been applied to nonlifting and lifting bodies of revolution in references 1 through 4. It was found that the generalized shock-expansion method accurately predicted the flow about pointed bodies of revolution when the hypersonic similarity parameter (ratio of Mach number to body fineness ratio) was greater than about 1. This method is, therefore, particularly useful in the treatment of flows about bodies traveling at relatively large Mach numbers. At lower speeds, the second-order potential theory of Van Dyke (ref. 5) has been widely used. (See, also, his hybrid theory for slightly inclined bodies, ref. 6.) The application of this theory to bodies traveling at large Mach numbers is often limited, however, by the restriction that the maximum slope of the body must be somewhat less than the slope of a free-stream Mach line.

The ranges of applicability of the generalized shock-expansion method and the second-order potential theory do not always overlap, and there remain, therefore, flows at certain combinations of Mach number and body shape which cannot be treated by either theory. Normally, these intermediate flows are encountered when the hypersonic similarity parameter based on nose fineness ratio is in the neighborhood of 1. Since this is a range of practical interest, additional theoretical methods are needed. Some of this need has been fulfilled by the hypersonic small-disturbance theory (refs. 7 and 8). In its present state of development, however, this theory has application only to limited classes of noninclined bodies of revolution. For example, due to the series form used to represent the pressure distribution, it cannot be applied to the nose-cylinder combinations commonly employed for missile bodies. In large part, then, the need for a theory applicable at values of the hypersonic similarity parameter near 1 still remains.

The present report develops a theory intended to fulfill this need. It is developed by an iteration procedure which employs the generalized method of references 1 through 4 as the first approximation. This theory is therefore called a second-order shock-expansion method. Expressions are derived which define the pressures on noninclined bodies of revolution. Expressions are also obtained for the normal-force and pitching-moment derivatives at zero angle of attack. Predictions of the method are compared with those of other theories and with experimental results.

SYMBOLS

A	body cross-sectional area
A_B	body base area
B	function defined by equation (B15)
C_1, C_2	characteristic coordinates
C_N	normal-force coefficient, $\dfrac{\text{normal-force}}{q_\infty A_B}$
C_m	pitching-moment coefficient, $\dfrac{\text{moment about body vertex}}{q_\infty A_B d}$
C_p	pressure coefficient, $\dfrac{p - p_\infty}{q_\infty}$
d	body diameter
E	entropy
f	fineness ratio (Fineness ratio of the nose section is f_n.)
l	body length
M	Mach number
p	static pressure
p_t	total pressure
q	dynamic pressure
s, n	rectangular coordinates (streamline direction and normal to streamline direction, respectively)
x, r, φ	cylindrical coordinates (x measured from vertex of body and φ from windward meridian)
$\bar{x}$	center-of-pressure position (measured from body vertex)
α	angle of attack, radians
β	function defined by equation (12)
γ	ratio of specific heats (1.400 for air)
δ	flow deflection angle
η	function defined by equation (9)
Λ	loading (defined by eq. (14))
λ	function defined by equation (B16)
μ	Mach angle (arc sine $1/M$)
ν	Prandtl-Meyer expansion angle
σ	shock-wave angle
ψ	function defined by equation (13)
Ω	ratio of cross-sectional area of streamtube to that at $M = 1$ (see eq. (B17))

SUBSCRIPTS

∞	free-stream conditions
1, 2, 3, 4,	conditions evaluated at various points in flow field
a	afterbody
c	quantities evaluated for cone tangent to the body
s	quantities evaluated by generalized shock-expansion method
v	quantities evaluated at vertex of body
σ	quantities evaluated along downstream face of shock wave
tcv	quantities evaluated for cones tangent to body vertex
tcx	quantities evaluated for cones tangent to body at station x

THEORY

In the present development of a second-order shock-expansion method, attention will be restricted to bodies of revolution. It is recognized, however, that the procedure used herein may, in the future, find application to other three-dimensional shapes.

The present method is a refinement of the generalized shock-expansion method of references 1 through 4. On the surface of a body of revolution, immediately behind a corner, the generalized method represents a first-order solution for the flow and the present method gives the second-order solution (see Appendix A). Before proceeding, therefore, it is well to orient the present analysis with a review of the approximations involved in the treatment of the flow about bodies of revolution with the generalized method. These approximations may be listed as follows (see, e. g., ref. 4): (1) Disturbances incident on an oblique shock wave are largely absorbed therein, and hence, reflected disturbances are negligible; (2) the flow appears locally two-dimensional; (3) surface streamlines may be taken as meridian lines. In the intermediate range of supersonic speeds of interest here, the first approximation is particularly well justified (see, ref. 9), and it will not be considered further. As a consequence of the second approximation, a solution given by the generalized method satisfies the continuity equation only approximately.[2] Although the continuity equation does not appear explicitly in the following analysis, it is this approximation that is refined by the present method. The third approximation applies only to inclined bodies of revolution, since for noninclined bodies, meridian lines are, of course, the exact streamlines. In the present investigation, attention will be restricted to bodies near zero lift. Under this restriction to infinitesimal angles of attack, an analysis has shown that the deviation of true streamlines from meridian lines has negligible effect on surface pressures. In the following development, therefore, the use of meridian lines as streamlines will be retained.

NONLIFTING BODIES

The generalized shock-expansion method was developed for nonlifting bodies of revolution from the method of characteristics (ref. 2). This development may be summarized with the aid of the equation for the streamwise pressure gradient (see, e. g., refs. 2 and 9).

$$\frac{\partial p}{\partial s} - \frac{2\gamma p}{\sin 2\mu} \frac{\partial \delta}{\partial s} = \frac{1}{\cos \mu} \frac{\partial p}{\partial C_1} \tag{1}$$

In the generalized method the pressure is considered constant along first-family Mach lines (refs. 1 and 4). As a consequence, the right-hand member of equation (1) is approximated by zero, and the equation can be integrated to yield the well-known Prandtl-Meyer relation. The objective of the present analysis is to refine this approximation to the right-hand member of equation (1). To this end, consider the flow about a body of revolution which has a pointed nose and over which the flow is everywhere supersonic. The problem will be simplified by approximating the profile of the body with a series of tangents to the original contour (see fig. 1). It might be noted that Ferrari (ref. 10) suggested a similar scheme with a body whose profile was made up of chord lines joining points on the original contour. While either approximation is permissible, the tangent body was selected here so that the conical flow at the vertex will

---

[2] In the treatment of two-dimensional flows, the first approximation is used but continuity is exactly satisfied.
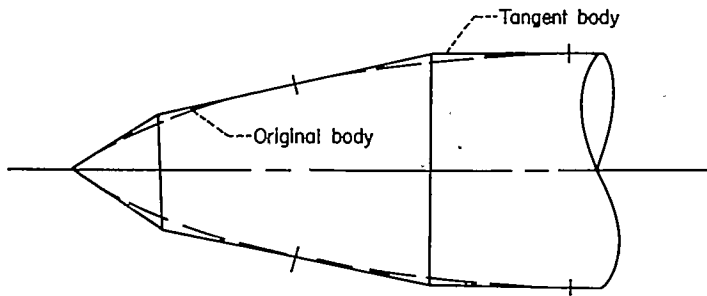
FIGURE 1.—Approximation of body shape by a tangent body.

be correct regardless of the degree of approximation used downstream of the vertex.

The generalized method gives the exact change in surface pressure around the corners of the tangent body but predicts no change along the straight-line elements. The present problem reduces to the determination of the pressure variation along the conical frustums.

Since along these surfaces $\partial\delta/\partial s=0$, equation (1) has the form

$$\frac{\partial p}{\partial s}=\frac{1}{\cos\mu}\frac{\partial p}{\partial C_1} \qquad (2)$$

The problem now is to find an approximation to the right-hand member of this equation. One approximation is a power series in s. Such an approximation would yield, of course, the surface pressure as a function of s, and thus, the power series could be written equally well in terms of pressure, p. For reasons which will become apparent later in the analysis, a combination of the two series will prove advantageous. Thus, the pressure gradient will be written

$$\frac{\partial p}{\partial s}=(P_0+p)(S_0+S_1s+S_2s^2+\dots)$$

where P_0 and S_n are constants for a particular frustum element. This equation is readily integrated to yield an exponential variation in pressure [3]

$$p=-P_0+Ce^{\left(S_0s+S_1\frac{s^2}{2}+S_2\frac{s^3}{3}+\dots\right)} \qquad (3)$$

where C is the constant of integration. Conditions must now be sought to evaluate the constants in this equation. For this purpose, the flow over a single conical-frustum element, such as shown in figure 2, will be considered. The
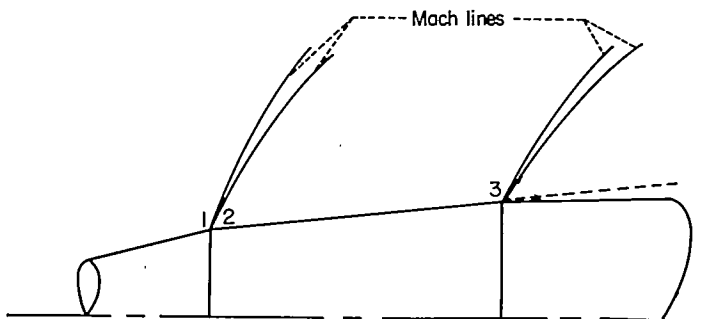

FIGURE 2.—Flow about a frustum element.

[3] It might be noted that Ehret, Rossow, and Stevens (ref. 11) found that pressures on ogives correlated according to the hypersonic similarity law could be represented approximately by an exponential function of distance.

subscript 1 will be employed to designate conditions immediately upstream of the corner preceding the frustum; the subscript 2, conditions immediately downstream of the corner; the subscript 3, conditions at the downstream end of the frustum. The first boundary condition to be applied is relatively obvious, and it is

$$p=p_2 \text{ at } s=s_2$$

Thus equation (3) becomes

$$p=-P_0+(p_2+P_0)e^{\left[S_0(s-s_1)+S_1\frac{(s-s_1)^2}{2}+S_2\frac{(s-s_2)^3}{3}+\dots\right]} \qquad (4)$$

It is also apparent that, if the conical element shown in figure 2 were extended indefinitely downstream rather than ending at point 3 (see dashed line in fig. 2), then the pressure on this extended surface would approach some limiting value. If the element were considered to be infinitely long, then the only effect the flow upstream of point 2 will have on the flow at infinity is to produce an infinitesimally thin layer on the surface across which the entropy varies. It is readily demonstrated, however, that there is no change in pressure across this layer and that the flow outside the layer is conical. Thus, a second boundary condition is

$$p\rightarrow p_c \text{ as } s\rightarrow\infty$$

where p_c is the pressure on a cone tangent to the original body at the same point as the frustum element. This condition gives the result

$$P_o=-p_c \qquad (5)$$

provided, of course, the constants, S_n, are negative. These constants, S_n, are now all that remain to be determined and they may be evaluated in terms of the various derivatives of pressure evaluated at point 2. Thus,

$$\left.\begin{array}{l} S_0=\dfrac{-\left(\frac{\partial p}{\partial s}\right)_2}{p_c-p_2} \\[2em] S_1=\dfrac{-\left(\frac{\partial^2 p}{\partial s^2}\right)_2}{p_c-p_2}-S_0{}^2 \\[2em] S_2=-\dfrac{1}{2}\left[\dfrac{\left(\frac{\partial^3 p}{\partial s^3}\right)_2}{p_c-p_2}+S_0{}^3+3S_0S_1\right] \end{array}\right\} \qquad (6)$$

at $s=s_2$ and so forth for additional terms.

At this point, it is well to comment on the choice of the series used to approximate the pressure gradient. For example, had the series been written entirely in terms of s, then a simple Taylor series for the pressure would have resulted. While the present approximation can be reduced to a Taylor series for small $(s-s_2)$, it has added features which are desirable. In particular, it is apparent that, within the framework of the approximation involved in the use of conical frustums rather than a curved body, the boundary conditions in pressure at both $s=s_2$ and $s\rightarrow\infty$ have been met exactly. It is primarily because of the particular choice of

series which led to the exponential form that it was possible to employ the boundary condition at $s \to \infty$. The meeting of this condition is relatively important from a practical viewpoint since it serves to limit the possible error involved in the use of a series approximation. For example, had a Taylor series been used and all boundary conditions applied at $s = s_2$, then the error for a given approximation could increase indefinitely with distance from the corner. With the approximation chosen, however, the error must be limited since at large s, the solution again becomes exact. This added accuracy is not obtained without incurring certain restrictions, however; since, as previously noted, the coefficients S_n must be negative. This condition must be satisfied for the present results to be applicable.

In the following analysis, only the first term, S_o, in the series will be retained, and thus only the first derivative of the pressure at point 2 will be required (see eq. (6)). As found in Appendix B, an expression defining this gradient is

$$\left(\frac{\partial p}{\partial s}\right)_2 = \frac{B_2}{r}\left(\frac{\Omega_1}{\Omega_2}\sin \delta_2 - \sin \delta_2\right) + \frac{B_2}{B_1}\frac{\Omega_1}{\Omega_2}\left(\frac{\partial p}{\partial s}\right)_1 \quad (7)$$

where

$$B = \frac{\gamma p M^2}{2(M^2-1)}$$

and Ω is the one-dimensional area ratio or

$$\Omega = \frac{1}{M}\left[\frac{1+\left(\frac{\gamma-1}{2}\right)M^2}{\frac{\gamma+1}{2}}\right]^{\frac{\gamma+1}{2(\gamma-1)}}$$

With the application of these results, the pressure along the conical frustum is given by

$$p = p_c - (p_c - p_2)e^{-\eta} \quad (8)$$

where

$$\eta = \left(\frac{\partial p}{\partial s}\right)_2\frac{x-x_2}{(p_c-p_2)\cos \delta_2} \quad (9)$$

It is apparent that, in order to apply equation (8), the pressure (and Mach number) on the surface of noninclined cones must be known. These quantities may be determined from the results of reference 2 or reference 12. For convenience, the surves shown in figure 3 have been plotted from the results of reference 12.

By application of equation (8) on successive elements, the pressure distribution on the tangent body can be determined. In particular, the pressure at each of the points of tangency may be calculated and applied to the original body. The procedure is as follows: First, the elements of the tangent body are selected and the coordinates (x,r) of each corner determined. The first element is tangent to the body at the vertex, and the flow over this element is thus conical. For the first corner, then, the pressure, p_1, and the Mach number, M_1 (see fig. 2), are the same as at the vertex of the original body. The pressure, p_2, and the Mach number, M_2, may then be determined with the Prandtl-Meyer equations. The pressure gradient, $(\partial p/\partial s)_2$,

may be determined from equation (7) since, for the first corner, $(\partial p/\partial s)_1$ is zero. The tangent-cone pressure, p_o, may be obtained from reference 12 or figure 3. With the various factors in equation (8) thus evaluated, the pressure at the tangent point and at point 3 (see fig. 2) can be calculated. In like manner, the pressure gradient at point 3 can be determined by differentiation of equation (8), or

$$\left(\frac{\partial p}{\partial s}\right)_3 = \left(\frac{p_c-p_3}{p_c-p_2}\right)\left(\frac{\partial p}{\partial s}\right)_2 \quad (10)$$

With the pressure and pressure gradient at point 3 known (the Mach number may also be calculated from the pressure in the usual manner), the factors in equation (8) may be determined for the next element. This process is, of course, repeated for each element of the tangent body.

The procedure just described is not difficult to apply; however, further simplification can be obtained by the use of a "two-step" tangent body. This body consists of a cone tangent to the original body at the vertex and a conical surface tangent to the body at the station where the pressure is to be calculated. With this two-step body, the second surface is a variable depending on the station in question on the original body. For this approximation, equation (8) becomes

$$p = p_c - (p_c - p_s)e^{-\beta \psi} \quad (11)$$

where

$$\beta = \frac{x \sin \delta_s - r \cos \delta_s}{r \cos \delta - x \sin \delta} \quad (12)$$

$$\psi = \frac{B_s}{(p_c-p_s)}\left(\frac{\Omega_s}{\Omega_s} - \frac{\sin \delta}{\sin \delta_s}\right) \quad (13)$$

The subscript, s, denotes quantities at the station on the body as evaluated by the generalized shock-expansion method. With equation (11) it is possible to obtain, very rapidly, a first approximation to the pressure distribution.

The second-order shock-expansion method has been developed to predict the pressures on a noninclined body of revolution. In the following section this method will be extended to lifting bodies.

LIFTING BODIES

For inclined bodies of revolution, a second-order shock-expansion method would involve not only a revised expression for the pressures, but, in addition, a revised approximation to the shape of the surface streamlines. It is recalled from the results of Eggers and Savin (ref. 1) that, according to the generalized method, surface streamlines may be approximated by geodesics. For bodies of revolution, the pertinent geodesics are simply meridian lines (refs. 1 and 3). While this result is exact for noninclined bodies of revolution, it is only an approximation in the case of inclined bodies. A refined approximation corresponding to a second-order method undoubtedly could be obtained by graphical integration of the momentum equations employing the pressure distribution given by the generalized method. However, it seems at present that this procedure would involve extensive calculations. If attention is restricted to bodies near $\alpha = 0$, it can be demonstrated that the deviation of the true streamlines from the meridian lines will not influence
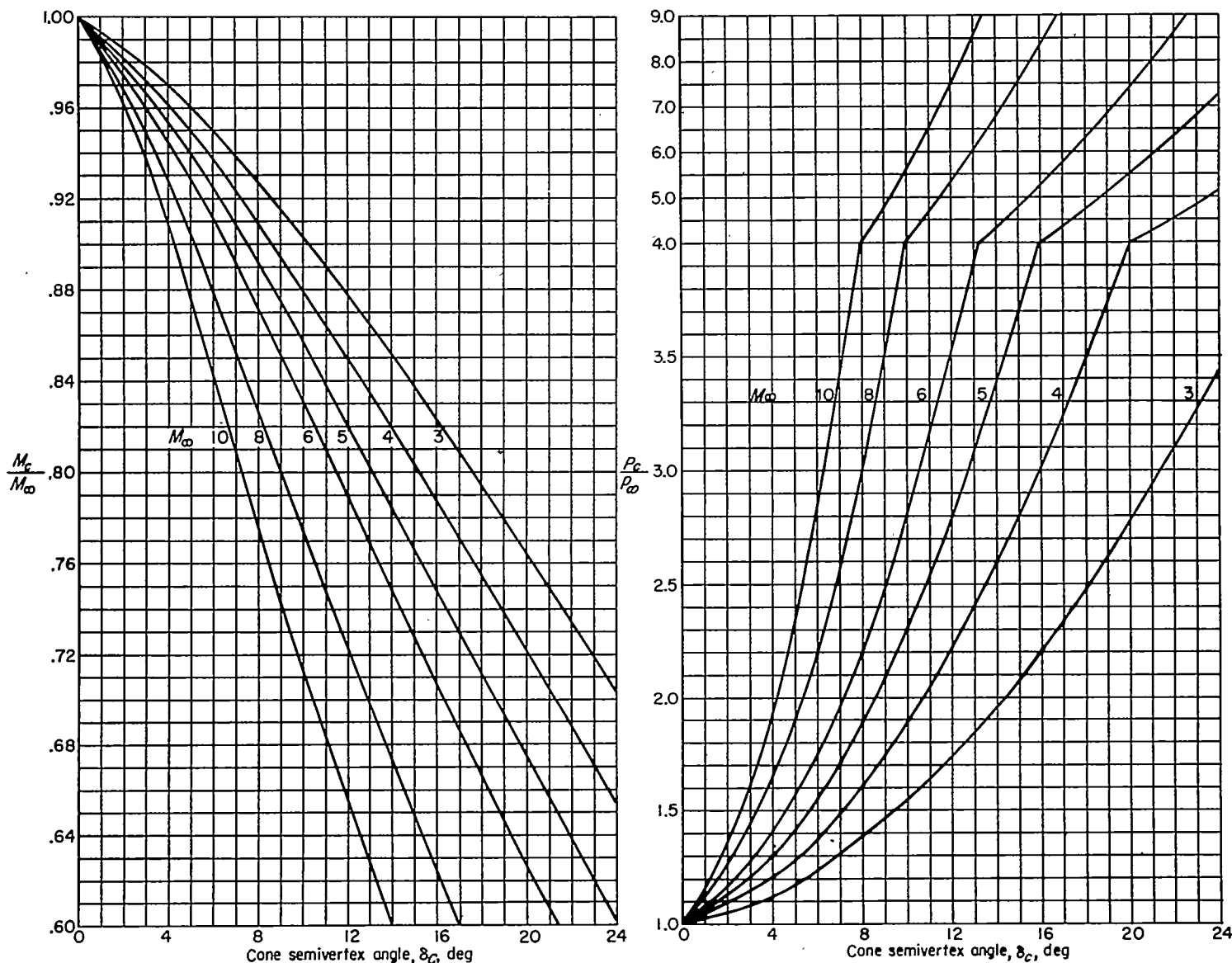
FIGURE 3.—Curves defining Mach number and pressure on the surface of noninclined cones (ref. 12).

surface pressures. The approximation of meridian lines as streamlines can, in effect, be retained and relatively simple expressions can be obtained, therefore, for the initial slopes of the normal-force and pitching-moment curves. To this end, the expression for the normal-force derivative can be written

$$\frac{dC_N}{d\alpha} = \frac{2\pi}{A_B} \int_0^l \Lambda r \, dx \qquad (14)$$

where the subscript, $\alpha=0$, has been omitted for simplicity of notation and where Λ is the nondimensional loading on a thin disk normal to the body axis and having unit radius. This loading Λ is given by the equation

$$\Lambda = \frac{2}{\gamma M_\infty^2 \pi} \int_0^\pi \frac{d(p/p_\infty)}{d\alpha} \cos \varphi \, d\varphi \qquad (15)$$

The problem then is to evaluate $d(p/p_\infty)/d\alpha$. The development given previously which led to equation (3) also applies to bodies at infinitesimal angles of attack. Equation (8) also applies; however, the variables in this equation must be

considered as dependent on angle of attack. By differentiation of equation (8), there is obtained

$$\frac{d(p/p_\infty)}{d\alpha} = (1-e^{-\eta}) \frac{d(p_c/p_\infty)}{d\alpha} + e^{-\eta} \frac{d(p_2/p_\infty)}{d\alpha} + (p_c - p_2) e^{-\eta} \frac{d\eta}{d\alpha} \qquad (16)$$

This equation must satisfy the condition $\dfrac{d(p/p_\infty)}{d\alpha} = \dfrac{d(p_2/p_\infty)}{d\alpha}$ at $\eta=0$ (i. e., $x=x_2$). By the application of this condition to equation (16), the last term (involving $d\eta/d\alpha$) is eliminated. The term, $d(p_2/p_\infty)/d\alpha$ may be evaluated with the aid of the Prandtl-Meyer equation

$$\frac{d(p_2/p_\infty)}{d\alpha} = \frac{\lambda_2}{\lambda_1} \left[\frac{d(p_1/p_\infty)}{d\alpha} - \frac{p_1}{p_\infty} \frac{1}{p_{t_1}} \frac{d(p_{t_1})}{d\alpha} \right] + \frac{p_2}{p_\infty} \frac{1}{p_{t_2}} \frac{d(p_{t_2})}{d\alpha} \qquad (17)$$

Ferri (ref. 13) has shown that the entropy (and hence the total pressure, p_t) on the surface of an inclined cone is constant (independent of φ). When equations (15), (16), and (17) are combined, then, the integrals of the terms involving $dp_{t_1}/d\alpha$ and $dp_{t_2}/d\alpha$ will be zero (since $\int_0^\pi \cos \varphi \, d\varphi = 0$).

Equation (15) may therefore be written

$$A=\frac{2}{\gamma M_\infty^2 \pi}\int_o^\pi \left[(1-e^{-\eta})\frac{d(p_c/p_\infty)}{d\alpha}+e^{-\eta}\frac{\lambda_2}{\lambda_1}\frac{d(p_1/p_\infty)}{d\alpha}\right]\cos\varphi\,d\varphi \quad (18)$$

The only terms in equation (18) that are functions of φ are $d(p_c/p_\infty)/d\alpha$ and $d(p_1/p_\infty)/d\alpha$. These two terms may be evaluated in terms of the normal-force derivative of the tangent cone, $\frac{dC_N}{d\alpha}\Big|_{tc\alpha}$, and in terms of A_1. After performance of the necessary manipulations, there is obtained

$$A=(1-e^{-\eta})(\tan\delta)\frac{dC_N}{d\alpha}\Big|_{tc\alpha}+\frac{\lambda_2}{\lambda_1}e^{-\eta}A_1 \quad (19)$$

It is apparent from equation (19) that $dC_N/d\alpha$ for cones must be known before the loading, A, can be evaluated. Fortunately, results for cones are available from reference 14 and have been plotted for convenience in figure 4. The loading, A, may thus be calculated in the same manner as the zero-lift pressures. In this case, A_1 for the first corner is simply $(\tan\delta_v)\frac{dC_N}{d\alpha}\Big|_{tc_v}$.
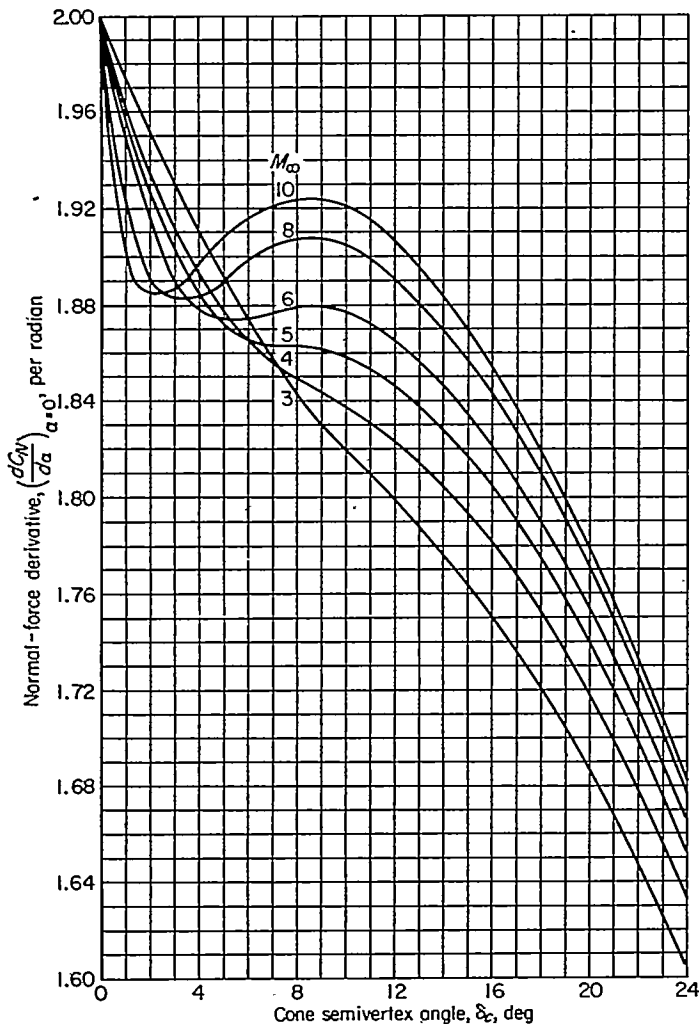

FIGURE 4.—Normal-force derivative $\left(\frac{dC_N}{d\alpha}\text{ at }\alpha=0\right)$ for cones (ref. 14).

As before, a first approximation to A can be obtained with the two-step body. This approximation gives

$$A=(1-e^{-\beta\psi})(\tan\delta)\frac{dC_N}{d\alpha}\Big|_{tc\alpha}+\left(\frac{\lambda_2}{\lambda_1}\right)(e^{-\beta\psi})(\tan\delta_v)\frac{dC_N}{d\alpha}\Big|_{tc_v} \quad (20)$$

In Appendix C, it is shown that equation (20) leads to very simple results for certain common body shapes.

With the loading, A, known, the normal-force derivative may be evaluated by integration of equation (14). In like manner, the pitching-moment derivative can be determined from the equation

$$\frac{dC_m}{d\alpha}=\frac{-2\pi}{A_B d}\int_o^l A r x\,dx \quad (21)$$

where the contribution to the pitching moment of the variation in local axial forces with angle of attack has been neglected since it is small for slender bodies (see ref. 15).

A second-order shock-expansion method for bodies of revolution has been developed to predict the pressure distribution and the normal-force and pitching-moment derivatives at $\alpha=0$. The results are relatively simple in form and may be applied to a given body with only a moderate amount of computations required. Simplified expressions based on an additional approximation have also been presented which further reduce the amount of work required. It should be noted, however, that open-nosed bodies and pointed bodies which produce shock waves other than the one at the vertex require special forms of the method. The necessary equations for these cases are contained in Appendix B. In addition, there are several restrictions on the present method which should be mentioned. First, it is apparent that if the exponential variation of the pressures is to be valid, then the pressure gradient just downstream of the corner must have the same sign as the pressure difference p_c-p_2. This condition, which derives from the previously noted restriction that the constants, S_n, in equation (4) be negative, is given by $\eta\geq0$ in the general case and by $\psi\geq0$ for the simplified method. There is an additional restriction on the simplified method, and that is that the two-step bodies must be real bodies (i. e., the intersection of the two tangent lines must not occur at negative values of x or r). This condition is given by $\beta\geq0$. When $\eta=0$ or $\beta\psi=0$, all equations reduce to those given by the generalized shock-expansion method.

It remains, of course, to determine the accuracy of the second-order shock-expansion method and to define its range of applicability. There are sufficient data available, both from experiment and from characteristic solutions, with which the predictions of the method for zero-lift pressure distributions can be compared. However for the case of lifting bodies, sufficient data are not available, and for this reason, the experiments next discussed were conducted.

EXPERIMENT

An experimental program was conducted to determine the initial slopes of the normal-force curves and the centers of pressure for a series of nose-cylinder combinations. The tests were designed, of course, to permit a check on the

accuracy of the predictions of the second-order shock-expansion method just developed. It is recalled that the method is intended for application at values of the hypersonic similarity parameter, M_∞/f_n in the neighborhood of 1. The tests cover a range of M_∞/f_n from 0.43 to 2.09.

APPARATUS AND TESTS

The tests were conducted in the Ames 10- by 14-inch supersonic wind tunnel at Mach numbers of 3.00, 4.24, 5.05, and 6.28. For a detailed description of this wind tunnel and its aerodynamic characteristics, see reference 16. Normal forces and pitching moments for the test models were measured with a strain-gage balance. The balance consisted of a model support sting on which the moments were measured at four points. From these four measurements, the normal forces and centers of pressure were determined and checked. Measurements were made at nine angles of attack from $-2°$ to $+4°$ at each test Mach number. At each angle of attack, the values of $\bar{x}/d$ and C_N/α were calculated. These values were plotted as a function of angle of attack, and the intercepts at $\alpha=0$ of the resulting curves gave the values of $dC_N/d\alpha$ and $\bar{x}/d$ at $\alpha=0$.

Wind-tunnel calibration data (see ref. 16) were employed in combination with stagnation-pressure measurements to obtain the stream dynamic pressures. Reynolds numbers based on the maximum diameter of the models were

Mach number	Reynolds number million
3.00	0.79
4.24	.72
5.05	.35
6.28	.15

MODELS

Cones and circular-arc tangent ogives of fineness ratios 7, 5, and 3 were tested alone and with cylindrical afterbodies having lengths of 2, 4, 6, and 10 diameters. The models were made of polished steel and each had a base diameter of 1 inch.

ACCURACY OF TEST RESULTS

Stream Mach numbers in the region of the test bodies did not vary more than ±0.03 from the mean values at Mach numbers up to 5.05. A maximum variation of ±0.05 existed at the highest test Mach number of 6.28.

The accuracy of the test results is influenced by uncertainties in the measurement of moments and in the determination of the stream dynamic pressure and angle of attack. These uncertainties resulted in estimated maximum errors in the normal-force derivatives and centers of pressure as shown in the following table:

M_∞	$dC_N/d\alpha$	$\bar{x}/d$
3.00	±0.15	±0.10
4.24	$\pm.15$	$\pm.10$
5.05	$\pm.20$	$\pm.15$
6.28	$\pm.25$	$\pm.20$

It should be noted that, for the most part, the experimental results presented herein are in error by less than these estimates.

RESULTS AND DISCUSSION

NONLIFTING BODIES

The second-order shock-expansion method has been developed primarily to treat flows characterized by values of M_∞/f_n near unity. Accordingly, the method has been employed to obtain the zero-lift pressure distributions at $M_\infty/f_n=1$ for several different body shapes. In this and all subsequent applications of the present method to curved bodies, the tangent bodies employed were formed by elements tangent to the original bodies at stations $x/l_n=0$, 0.1, 0.2, . . . , 1.0. The tangent-body approximation is required only if the body profile is curved since for cone-cylinders, and for the cylindrical section of any nose-cylinder combination, the present method yields results in closed form.

The results of these calculations are shown in figure 5 along with distributions obtained with the generalized shock-
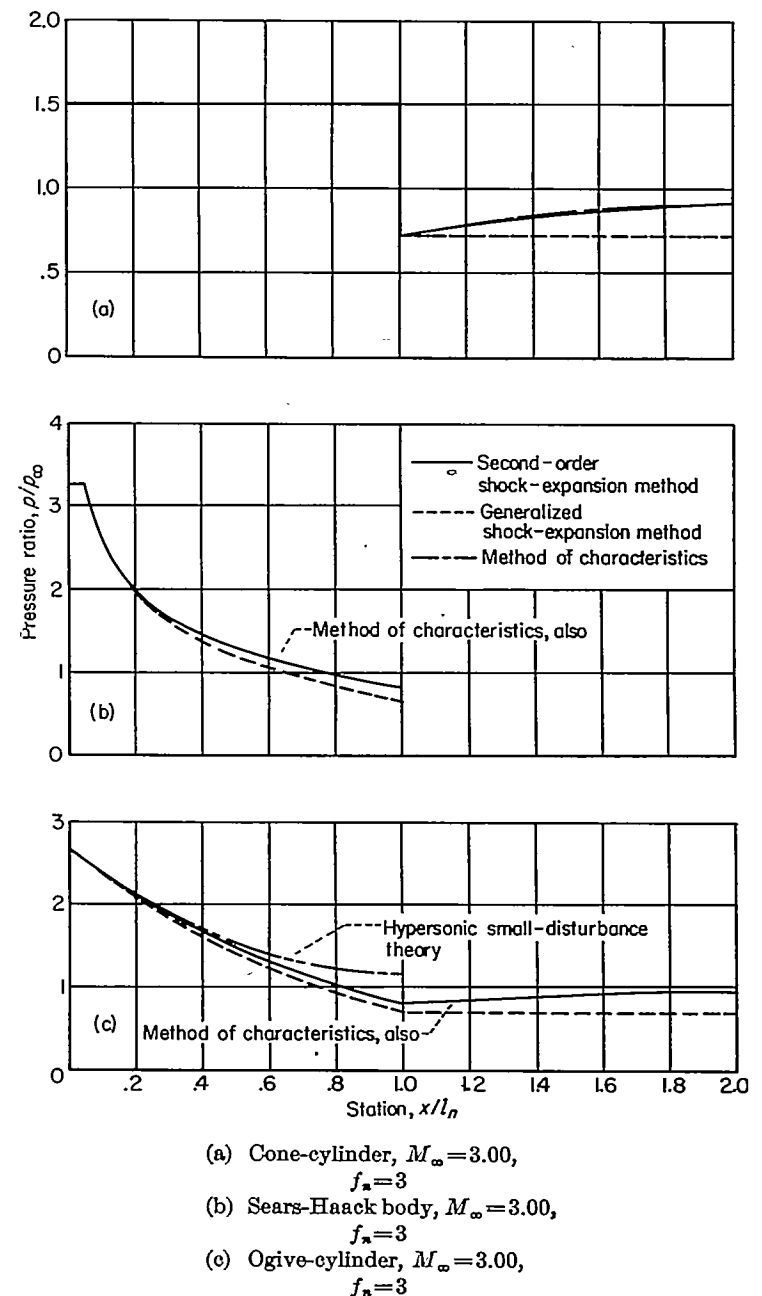

(a) Cone-cylinder, $M_\infty=3.00$, $f_n=3$
(b) Sears-Haack body, $M_\infty=3.00$, $f_n=3$
(c) Ogive-cylinder, $M_\infty=3.00$, $f_n=3$

FIGURE 5.—Surface-pressure distributions for various bodies at $M_\infty/f_n=1$ and $\alpha=0$.

expansion method (ref. 2). Distributions obtained with the method of characteristics (refs. 11, 17, and 18), which are considered to be exact, are also shown. It is apparent in figure 5 that the present method provides an improvement over the generalized method. The differences in the distributions obtained with the present method and those obtained with the method of characteristics are almost indiscernible.

In figure 5 (c), comparison is also made with the predictions of the hypersonic small-disturbance theory (ref. 8). The curve shown was calculated by three terms of a power series representation of the pressure distribution. As noted in reference 8, additional terms will be required before this method will accurately predict the pressures on an ogive. The small-disturbance theory does have a certain advantage in simplicity for, if the coefficients of the series expansion are known, the pressure distribution can be calculated very easily. This advantage is partially offset by the restriction that the series method requires the body profile to have continuous derivatives up to the same order as the number of terms used in the series. With this restriction, the theory cannot be applied beyond the nose-cylinder juncture of the body (fig. 5 (c)).

To investigate the accuracy of the present method at values of M_∞/f_n other than 1, the comparisons shown in figure 6 have been made. Here, the predictions of the present method and those of the generalized method are compared with experimental results for fineness ratio 3 and 5 tangent ogives at Mach numbers of 3.00, 4.24, and 5.05. The values of M_∞/f_n range from 0.60 to 1.68. The experimental results were taken from reference 3. For all cases shown, the predictions of the present method are within the accuracy of the experimental data. It is also apparent that the predictions of the present method tend to approach those of the generalized method as M_∞/f_n becomes appreciably greater than 1. At $M_\infty/f_n=1.68$, for example, the predictions of the two methods differ only slightly.

In figure 6, comparison is also made with the second-order potential theory (ref. 5) for conditions where this theory is applicable (i. e, $M_\infty/f_n=0.60$ and 0.85). It is somewhat surprising that the present method is as accurate as the second-order potential theory even at the relatively low value of M_∞/f_n of 0.60.

The results presented in figures 5 and 6 indicate that the present method fulfills its intended purpose by providing an estimate of the pressures on noninclined bodies of revolution for values of M_∞/f_n near 1. At values of M_∞/f_n as low as 0.60 the present method provides results comparable in accuracy with those obtained with the second-order potential
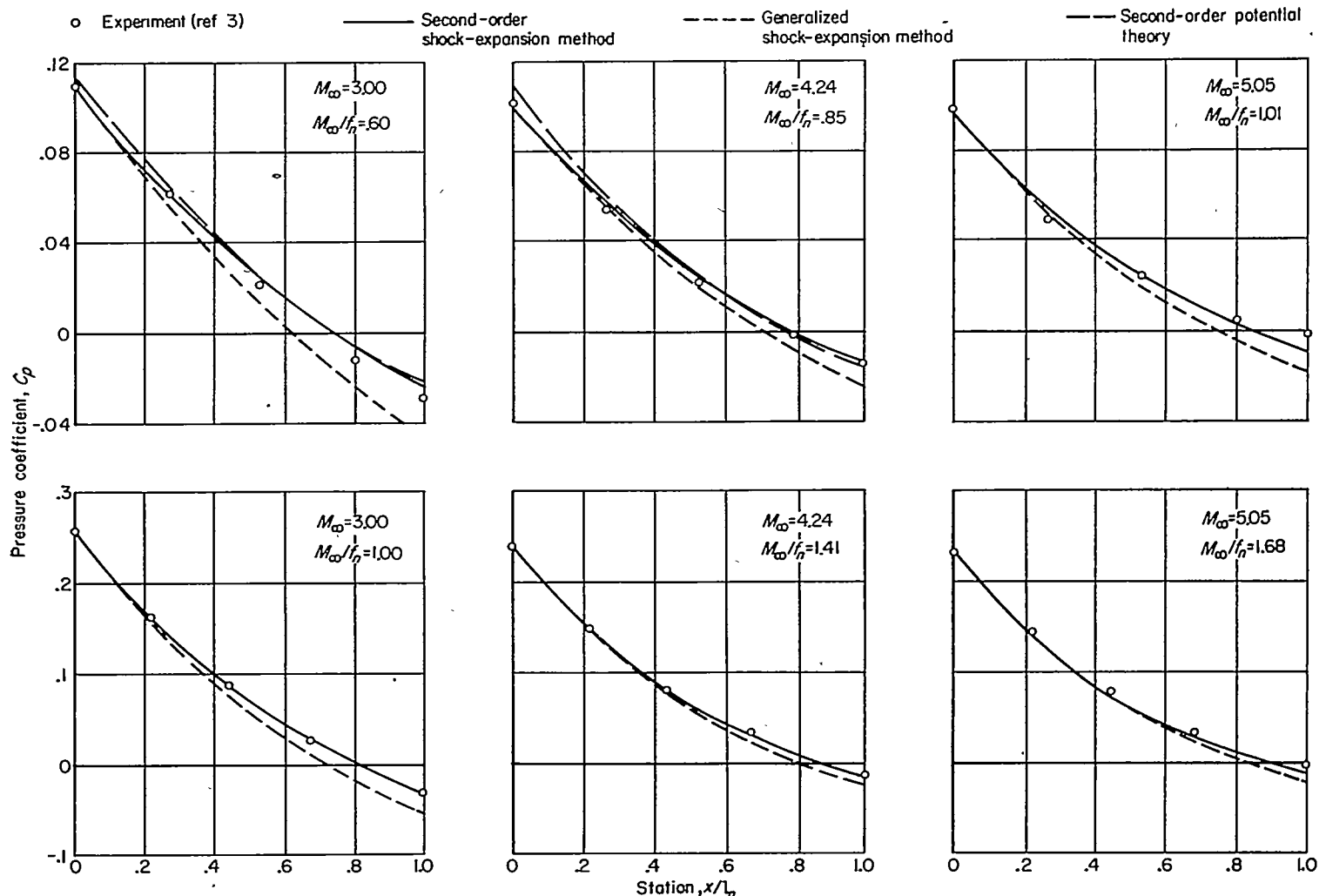

FIGURE 6.—Surface-pressure distributions for noninclined tangent ogives.

theory. At values of M_∞/f_n approaching 2, the predictions of the present method and those of the generalized shock-expansion method differ only slightly. It remains now to investigate the applications of the method to inclined bodies.

<div align="center">LIFTING BODIES</div>

The experimental results obtained in the present tests are given in tables I and II. Predictions of various theories are also tabulated. These include the predictions of the present method (with various approximations), the generalized shock-expansion method (ref. 3), first-order potential theory (refs. 6 and 19), Van Dyke's hybrid potential theory (ref. 6), and Newtonian impact theory (see, e. g., ref. 20). Solutions with the second-order potential theory employed in the application of the hybrid theory were obtained with the aid of reference 21. (Additional results obtained with the first-order and hybrid potential theories and with Newtonian impact theory may be found in reference 22.) With the exception of the two potential theories, all theories have been applied throughout the entire range of test variables. The potential theories cannot be employed, of course, if the free-stream Mach angle is less than the body semivertex angle.

Normal-force derivative.—The experimentally determined normal-force derivatives and the predictions of the various theories for the bodies tested are shown in figures 7 (a) through 7 (f). Curves for the first-order potential theory are not shown in figure 7 since, in all except a few cases, the predictions of this theory did not differ significantly from those of the hybrid potential theory (see tables I and II). In general, the present method predicts the normal-force derivatives at zero angle of attack essentially within the accuracy of the data (within about ± 0.2 per radian) throughout the entire range of test variables. In addition, the present method appears to provide the most consistently accurate results of all the theories presented in figure 7. The accuracy of the method at low values of M_∞/f_n can be explained partially by examination of the predictions of the method for the limiting case of very slender bodies. In this limit, it can be shown from equations (7) and (9) that the term, η, approaches infinity. From equation (19), then, the loading, Λ, may be written

$$\Lambda = 2\tan\delta = 2\frac{dr}{dx} \qquad (22)$$

since $\left.\dfrac{dC_N}{d\alpha}\right|_{tcr}=2$ (see fig. 4). With the substitution of this

equation in equation (14), there is obtained

$$\frac{dC_N}{d\alpha}=\frac{2\pi}{A_B}\int_0^l\left(2\frac{dr}{dx}\right)r\ dx=\frac{2}{A_B}\int_0^l\frac{dA}{dx}dx \qquad (23)$$

This result is, of course, the well-known prediction of slender-body theory, which is known to be accurate for slender bodies at low supersonic speeds. Thus, the accuracy of the present method at low values of M_∞/f_n can be attributed, in part, to the fact that it reduces to slender-body theory in the limit.

From the results given in figure 7, several observations can be made concerning the accuracy of other theories. For example, it might be expected that the potential theories would be more accurate than the other theories when the parameter $\sqrt{M_\infty{}^2-1}\tan\delta_v$ is appreciably less than 1. For the $f_n=7$ cone at $M_\infty=3$ (fig. 7 (a)), however, this parameter is only 0.20, and yet, for the longer afterbodies, the hybrid potential theory is appreciably more in error than the present method. As found in references 2 through 4, the generalized shock-expansion method gives accurate results when M_∞/f is greater than about 1. Caution should be expressed here, however, for the significant parameter is truly M_∞/f and not M_∞/f_n. The results shown in figure 7 indicate that although M_∞/f_n may be appreciably greater than 1, for cases where the afterbody is sufficiently long to reduce M_∞/f below 1, the predictions of the generalized method may depart appreciably from the experimental results. In general, impact theory gives acceptable results only for nose sections without afterbodies.

Center of pressure.—The experimentally determined centers of pressure and predictions of the various theories for the bodies tested are presented in figure 8. The present method predicts the location of the centers of pressure essentially within the accuracy of the data (within about ± 0.2 body diameters) throughout the entire range of test variables. In addition, the present method again provides the most consistently accurate results of all the theories presented. In general, all observations made previously regarding the reliability with which the various theories predict the normal-force derivatives can also be made in the case of the centers of pressure.

Ranges of applicability.—Several parameters are useful for defining the ranges of applicability of the various theories. The ranges of these parameters covered by the present tests are shown in the following table:

Parameter	Range
M_∞	3.00 to 6.28
f	3 to 17
f_n	3 to 7
f_a	0 to 10
M_∞/f	0.18 to 2.09
M_∞/f_n	0.43 to 2.09
$\sqrt{M_\infty{}^2-1}\tan\delta_v$	0.20 to 2.12

The second-order shock-expansion method was found to be applicable throughout the ranges of variables shown in the table. Both $dC_N/d\alpha$ and $\bar{x}/d$ were predicted within ± 0.2. The present tests did not reveal the limits of applicability of the method. It was indicated, however, that the method may apply to relatively low values of M_∞/f_n (or $\sqrt{M_\infty{}^2-1}\tan\delta_v$), since, in the limit of very slender bodies, the method reduces to the well-known slender-body theory. The upper limit of the method is dictated by the condition specified in the development—namely, $\eta\geq 0$ (see eq. (8)). Calculations have revealed that this condition will be violated if $\sqrt{M_\infty{}^2-1}\tan\delta_v$ is appreciably greater than 2.5. It should also be noted that the application of the present method to boattailed bodies presents a special problem
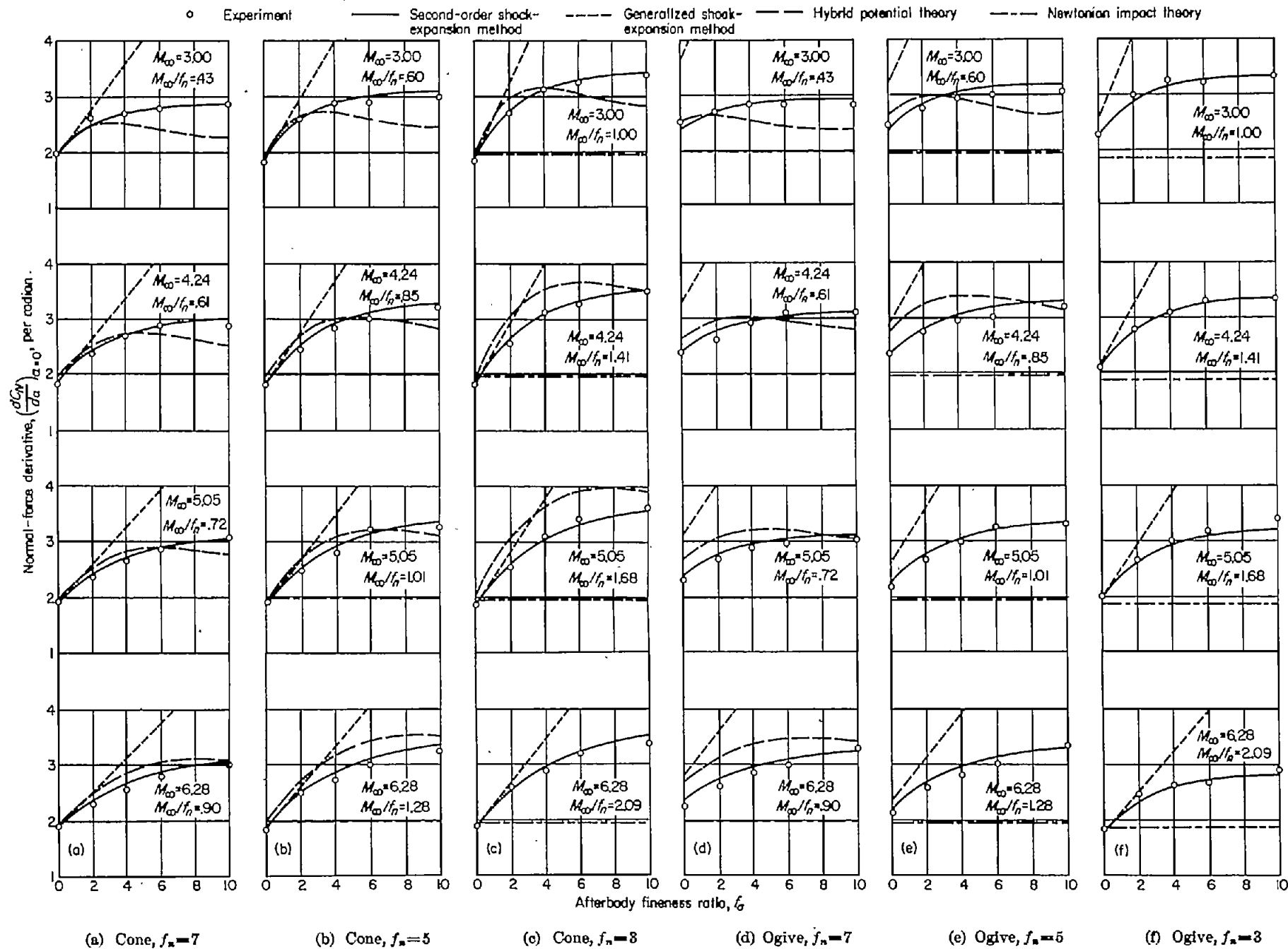
FIGURE 7.—Normal-force derivatives for various cone- and ogive-cylinders at Mach numbers from 3.00 to 6.28.

(a) Cone, $f_n = 7$ (b) Cone, $f_n = 5$ (c) Cone, $f_n = 3$ (d) Ogive, $f_n = 7$ (e) Ogive, $f_n = 5$ (f) Ogive, $f_n = 3$

(a) Cone, $f_n = 7$ (b) Cone, $f_n = 5$ (c) Cone, $f_n = 3$ (d) Ogive, $f_n = 7$ (e) Ogive, $f_n = 5$ (f) Ogive, $f_n = 3$
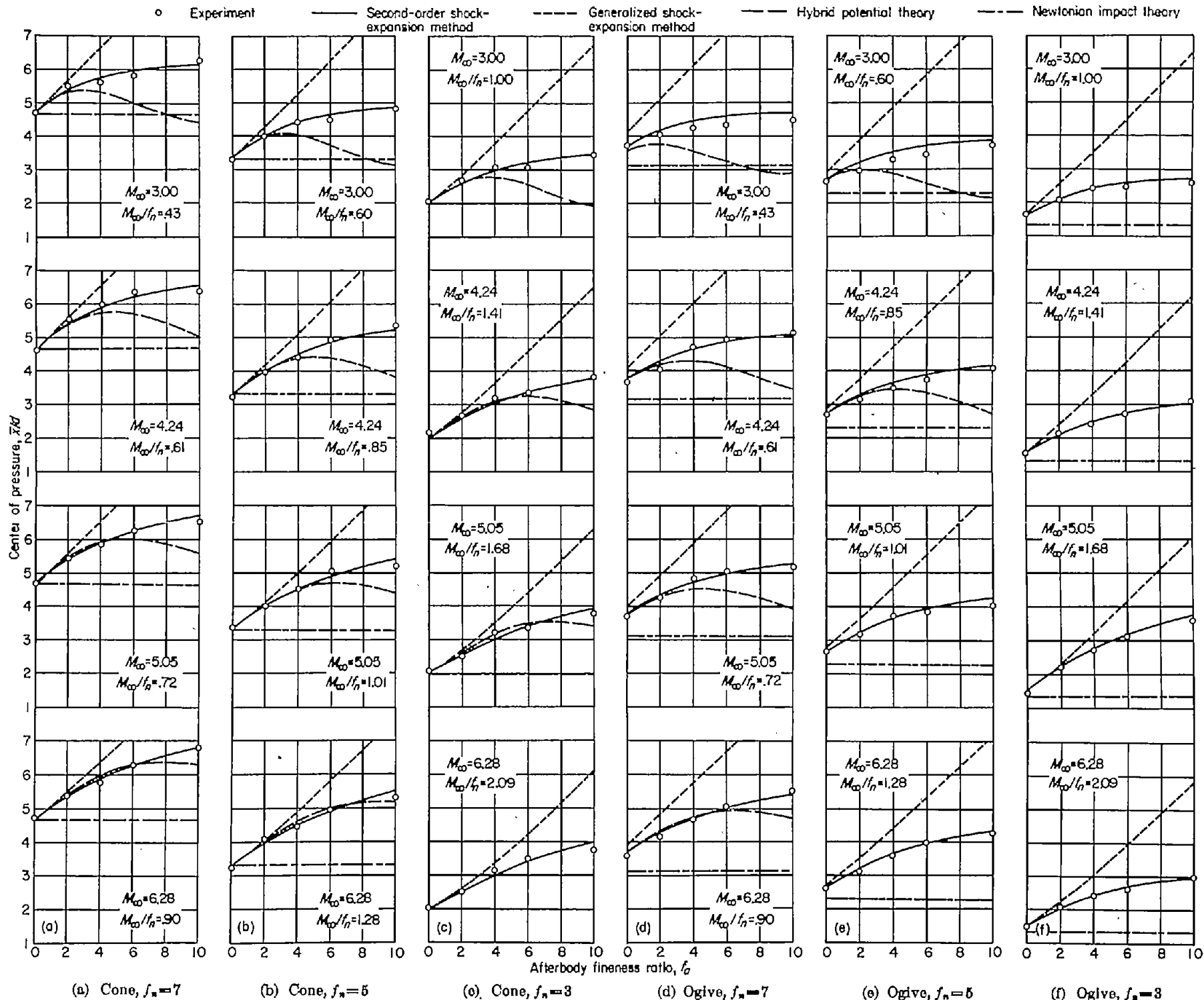
FIGURE 8.—Centers of pressure at $\alpha = 0$ for various cone- and ogive-cylinders at Mach numbers from 3.00 to 6.28.

since neither p_c nor $\left.\dfrac{dC_N}{d\alpha}\right|_{tcx}$ is defined in this case (see eqs. (8) and (20)). In practice, however, it has been found by comparison with results given in reference 23 that the use of $p_c = p_\infty$ and $\left.\dfrac{dC_N}{d\alpha}\right|_{tcx} = 2$ gives reasonable results for bodies having moderate amounts of boattail.

The present tests also reaffirmed the conclusion given in references 1 through 4, that the generalized shock-expansion method is applicable when M_∞/f is greater than about 1. At values of M_∞/f appreciably greater than 1, no significant differences between the predictions of the generalized and second-order methods were found. The ranges of applicability of these two methods overlap and thus include most flows about pointed bodies of revolution throughout the intermediate- and high-supersonic speed ranges.

Application of the potential theories is, of course, limited by the condition that $\sqrt{M_\infty{}^2-1}\,\tan\,\delta_v$ must be less than 1. Even at the lowest values of $\sqrt{M_\infty{}^2-1}\,\tan\,\delta_v$ covered by the present tests, however, neither the first-order nor the hybrid potential theory was found to provide consistently accurate predictions of $dC_N/d\alpha$ or $\bar{x}/d$. The calculations performed also revealed no significant differences in the predictions of the two theories at values of $\sqrt{M_\infty{}^2-1}\,\tan\,\delta_v$ less than about 0.7.

APPROXIMATIONS OF THE PRESENT METHOD

As noted in the development of the present method, a simplified solution for bodies with curved profiles can be obtained by the use of a two-step tangent body. This approximation has been applied to the ogive-cylinders of the present tests. By the use of additional approximations to the loading, Λ, the simplified solutions for $dC_N/d\alpha$ and $\bar{x}/d$ can be obtained in closed form as discussed in Appendix C. Examples of the accuracy of the approximate solutions are shown in figure 9. While the approximate methods do not yield results so consistently accurate as those obtained with a more complete solution, the approximate methods may still be useful to obtain rapid estimates of $dC_N/d\alpha$ and $\bar{x}/d$. In this connection, these quantities can be estimated for ogive-cylinders in a few minutes with the aid of the results given in Appendix C.

CONCLUSIONS

A second-order shock-expansion method applicable to bodies of revolution near zero lift has been developed. For noninclined bodies, the pressure distributions obtained with the method were compared with existing experimental results and with the predictions of other theories. For inclined bodies, the normal-force derivatives and centers of pressure at zero angle of attack determined with the method were compared with the predictions of other methods and
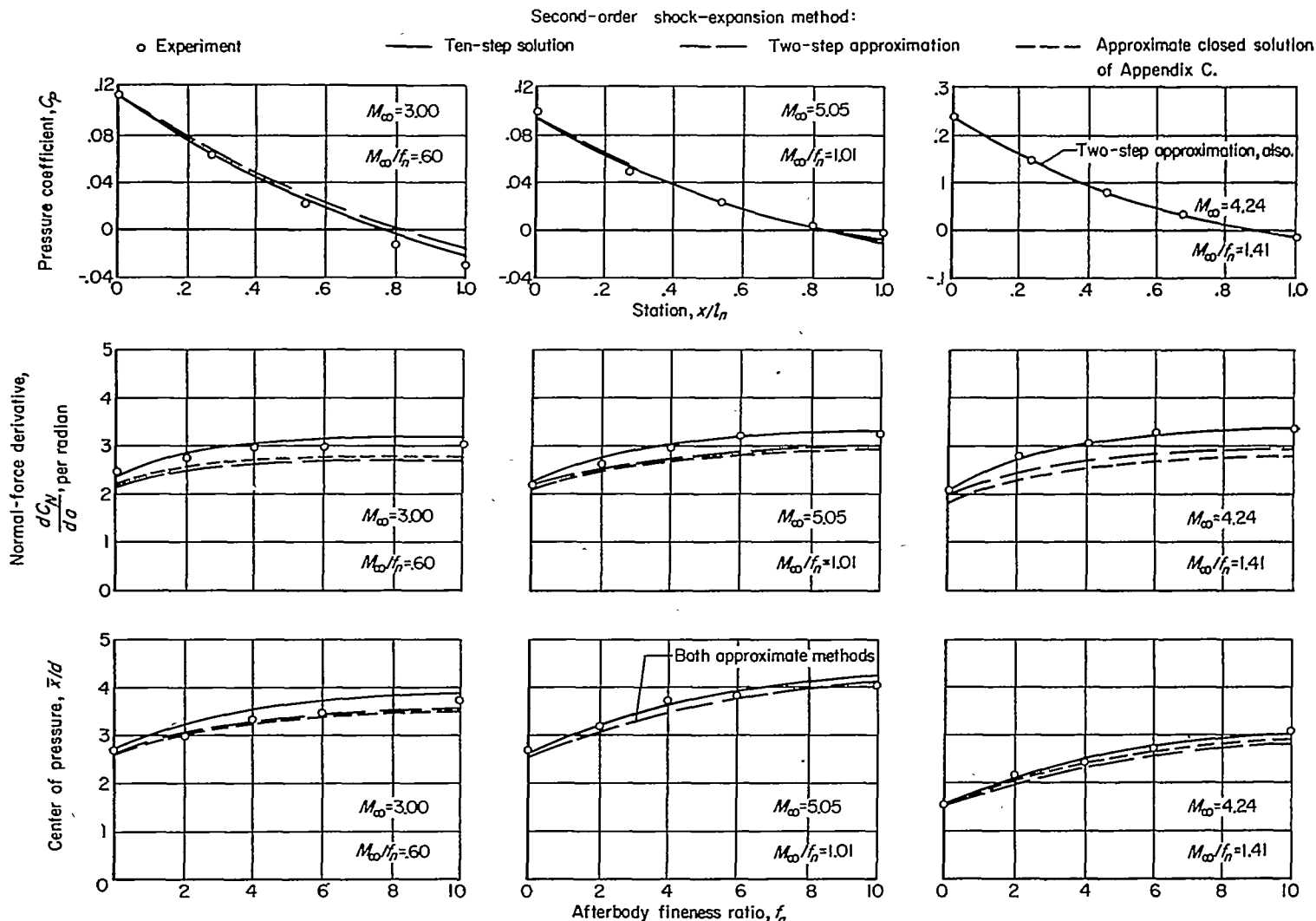

FIGURE 9.—Accuracy of approximate solutions for ogive-cylinders ($\alpha=0$).

with experimental results. Cone- and ogive-cylinders with fineness ratios from 3 to 17 were tested at Mach numbers from 3.00 to 6.28, corresponding to a range of values of the hypersonic similarity parameter based on nose fineness ratio (i. e., the ratio of free-stream Mach number to nose fineness ratio) from 0.43 to 2.09. These comparisons led to the following conclusions:

1. For noninclined bodies, the present method predicts the pressure distributions within the accuracy of experimental results. At values of the hypersonic similarity parameter based on nose fineness ratio as low as 0.6, the present method is as accurate as the second-order potential theory. At values of the parameter approaching 2, the predictions of

the present method differ only slightly from those of the generalized shock-expansion method.

2. For inclined bodies, the normal-force derivatives and the locations of the center of pressure at zero angle of attack predicted with the present method are in good agreement with the experimental results throughout the entire range of test variables. Within this range, the present method yields results more consistently accurate than those of other available theories.

AMES AERONAUTICAL LABORATORY
   NATIONAL ADVISORY COMMITTEE FOR AERONAUTICS
      MOFFETT FIELD, CALIF., *Oct. 12, 1955*

APPENDIX A

POWER SERIES REPRESENTATION OF FLOW ABOUT BODY OF REVOLUTION

The accuracy of the present method has been demonstrated by comparisons made over a wide range of flow parameters. It is also informative, however, to examine briefly the mathematical accuracy of the method. For this purpose, the model shown in figure 10 is useful. From the vertex to point 1, the body is conical. Between points 1 and 2, the surface is deflected by a small angle, ϵ. At any point downstream of point 1, the physical deviation of the body from a conical surface may be given in terms of the angle, ϵ, and the distance, Δs, measured from point 1. Similarly, flow parameters at any point downstream of point 1 may be expressed in terms of ϵ and Δs. Before developing such an expression, it should be noted that for this model (and within the restriction that the flow is everywhere supersonic), the present method provides an exact solution for the surface flow in several limits. For example, the present method is exact for all values of Δs when $\epsilon=0$. For $\Delta s=0$ and $\Delta s\rightarrow\infty$, the method is exact for all values of ϵ. For arbitrary values of Δs and ϵ, of course, the present method is not exact. However, the general accuracy of the method can be demonstrated by expressing flow parameters in the form of a Taylor series in the two independent variables, ϵ and Δs. The dependent variable used to define the flow may be any one of several parameters. Pressure and velocity are among those most commonly used. In the present analysis, however, the Prandtl-Meyer angle, ν, is considered the dependent variable. It should be recognized that the value of the Prandtl-Meyer angle at a point will define the Mach number,

pressure, velocity, and other such parameters. We have then the series

$$\nu=\nu_1+\left(\frac{\partial\nu}{\partial s}\right)_1(\Delta s)+\left(\frac{\partial\nu}{\partial\delta}\right)_1\epsilon+$$

$$\frac{1}{2!}\left[\left(\frac{\partial^2\nu}{\partial s^2}\right)_1(\Delta s)^2+2\left(\frac{\partial^2\nu}{\partial s\,\partial\delta}\right)_1(\Delta s)(\epsilon)+\left(\frac{\partial^2\nu}{\partial\delta^2}\right)_1(\epsilon^2)\right]+$$

$$\frac{1}{3!}\left[\left(\frac{\partial^3\nu}{\partial s^3}\right)_1(\Delta s)^3+3\left(\frac{\partial^3\nu}{\partial s^2\partial\delta}\right)_1(\Delta s)^2(\epsilon)+3\left(\frac{\partial^3\nu}{\partial s\,\partial\delta^2}\right)_1(\Delta s)(\epsilon^2)+$$

$$\left(\frac{\partial^3\nu}{\partial\delta^3}\right)_1(\epsilon^3)\right]+\ldots \tag{A1}$$

Each of the derivatives is evaluated at $\Delta s=\epsilon=0$. When $\epsilon=0$, it is apparent that the flow parameters are constant along the surface and independent of s. Therefore, all derivatives with respect to s alone are zero. When $\Delta s=0$, it is also apparent that $(\partial\nu/\partial\delta)_1=-1$ and that all higher derivatives with respect to δ alone are zero. We have then the problem of evaluating the cross derivatives. The second-order cross derivative, $(\partial^2\nu/\partial s\,\partial\delta)$, may be evaluated with the aid of equation (B14), from which $(\partial\nu/\partial s)_2$ may be determined; namely,

$$\left(\frac{\partial\nu}{\partial s}\right)_2=\frac{-1}{\lambda_2}\left(\frac{\partial p}{\partial s}\right)_2=\frac{-1}{2r_1\sqrt{M_2{}^2-1}}\left(\frac{\Omega_1}{\Omega_2}\sin\delta_1-\sin\delta_2\right) \tag{A2}$$

It is also apparent that

$$\left(\frac{\partial^2\nu}{\partial s\,\partial\delta}\right)_1=\frac{\partial}{\partial\delta}\left(\frac{\partial\nu}{\partial s}\right)_2 \tag{A3}$$

in the limit as $\delta_2\rightarrow\delta_1$. Hence, by virtue of equation (A2),

$$\left(\frac{\partial^2\nu}{\partial s\,\partial\delta}\right)_1=\frac{-\cos\delta_1}{2r_1\sqrt{M_1{}^2-1}}[(\sqrt{M_1{}^2-1}\tan\delta_1)-1] \tag{A4}$$

As noted in Appendix B, equation (B14) is not an exact solution for the pressure gradient since a term,

$$\frac{\lambda_2}{2\cos\mu_2}\int_4^5\frac{1}{\lambda\cos\mu}\left(\frac{\partial p}{\partial C_1}\right)\frac{ds}{b}$$
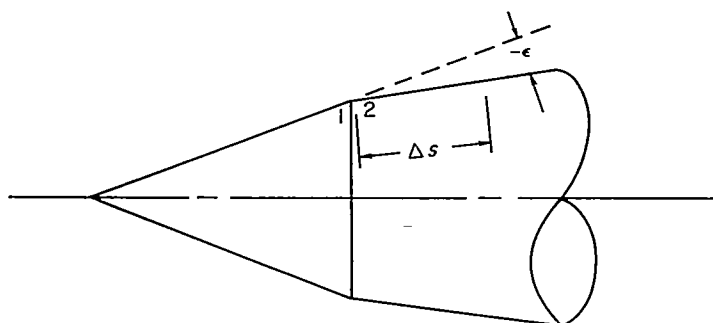
was neglected in the derivation (see eq. (B11)). In the

FIGURE 10.—Model for order analysis.

present analysis, both $\partial p/\partial C_1$ and the interval of integration, $(s_5-s_4)/b$ (see fig. 11), are of order ϵ; hence, the neglected term is of order ϵ^2. Equation (A2) is accurate to the first order in ϵ, therefore, and equation (A4) is exact. With the substitution of equation (A4) in equation (A1), and with the application of the other results previously noted, there is obtained

$$\nu = \nu_1 - \epsilon - \frac{\cos\delta_1}{2r_1\sqrt{M_1{}^2-1}}\left[\left(\sqrt{M_1{}^2-1}\,\tan\delta_1\right)-1\right](\Delta s)(\epsilon) +$$
$$0[(\Delta s)^2(\epsilon),(\Delta s)(\epsilon)^2] \quad \text{(A5)}$$

The generalized shock-expansion method of references 1 through 4 gives the result that $\nu=\nu_1-\epsilon$. The generalized method gives the Prandtl-Meyer angle mathematically accurate to the first order of the independent variables ϵ and Δs and, therefore, immediately downstream of the corner, gives a first-order solution for the surface flow. The present method adds the coefficient of the term involving (Δs) (ϵ) in equation (A5) and, hence, gives the Prandtl-Meyer angle

mathematically accurate to the second order of the independent variables ϵ and Δs. In general, therefore, immediately downstream of the corner the present method gives a second-order solution for the surface flow, and therefore, it has been termed the second-order shock-expansion method.

The foregoing analysis considered only expanding flows about the corner. If ϵ is positive, then the shock wave emanating from the corner must be considered. The result obtained is essentially the same, however. For positive ϵ a term of $0(\epsilon^3)$ must be added to equation (A5) to account for the difference between the Rankine-Hugoniot equations and the Prandtl-Meyer equations. Alternately, the term, $-\epsilon$, in equation (A5) can be replaced with the change in Prandtl-Meyer angle between points 1 and 2 as given by the Rankine-Hugoniot equations. The second-order term in either case is identical, however, as equation (A4) may also be obtained by differentiating equation (B21). (It may also be obtained by differentiation of the exact pressure-gradient equation, eq. (B18).)

APPENDIX B

EVALUATION OF PRESSURE GRADIENT DOWNSTREAM OF CORNER OF BODY OF REVOLUTION

CONVEX CORNER

Along a streamline in axially symmetric flow the following relation holds (see eq. (1))

$$\frac{\partial p}{\partial s}-\lambda\frac{\partial\delta}{\partial s}=\frac{1}{\cos\mu}\frac{\partial p}{\partial C_1}=\frac{-\lambda}{\cos\mu}\left(\frac{\partial\delta}{\partial C_1}+\frac{\sin\mu\sin\delta}{r}\right) \quad \text{(B1)}$$

From this equation, we may also write

$$\frac{\partial p}{\partial C_1}=\cos\mu\left(\frac{\partial p}{\partial s}-\lambda\frac{\partial\delta}{\partial s}\right) \quad \text{(B2)}$$

and

$$\frac{\partial\delta}{\partial C_1}=-\frac{\sin\mu\sin\delta}{r}-\frac{\cos\mu}{\lambda}\left(\frac{\partial p}{\partial s}-\lambda\frac{\partial\delta}{\partial s}\right) \quad \text{(B3)}$$

Consider now the flow in the region of a convex corner on a body of revolution as shown in figure 11. Between points 4 and 5, we may write,
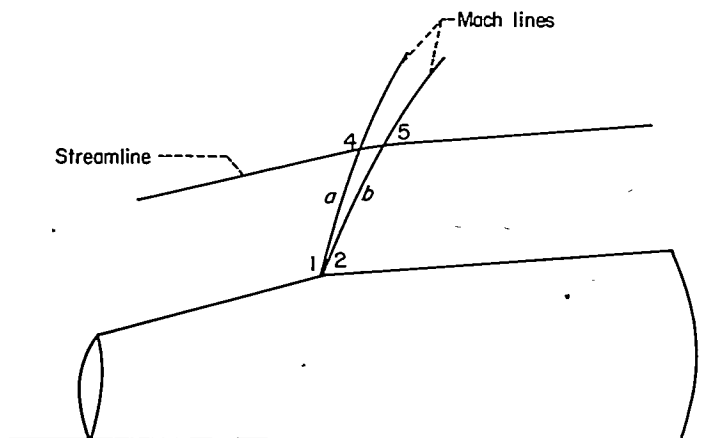
FIGURE 11.—Flow about a convex corner on a body of revolution.

from equation (B1)

$$\int_{p_4}^{p_5}\frac{dp}{\lambda}-(\delta_5-\delta_4)=\int_4^5\frac{1}{\lambda\cos\mu}\left(\frac{\partial p}{\partial C_1}\right)ds \quad \text{(B4)}$$

If points 4 and 5 are near to the surface, equation (B4) may be approximated by

$$\int_{p_1}^{p_2}\frac{dp}{\lambda}+\frac{p_5-p_2}{\lambda_2}-\frac{p_4-p_1}{\lambda_1}-(\delta_5-\delta_4)=\int_4^5\frac{1}{\lambda\cos\mu}\left(\frac{\partial p}{\partial C_1}\right)ds \quad \text{(B5)}$$

Since the flow between points 1 and 2 is strictly of the Prandtl-Meyer type,

$$\int_{p_1}^{p_2}\frac{dp}{\lambda}=\nu_1-\nu_2=\delta_2-\delta_1 \quad \text{(B6)}$$

We may also write from equations (B2) and (B3)

$$\frac{p_5-p_2}{\lambda_2}=\frac{1}{\lambda_2}\left(\frac{\partial p}{\partial C_1}\right)_2 b=\frac{\cos\mu_2}{\lambda_2}\left[\left(\frac{\partial p}{\partial s}\right)_2-\lambda_2\left(\frac{\partial\delta}{\partial s}\right)_2\right]b \quad \text{(B7)}$$

$$\frac{p_4-p_1}{\lambda_1}=\frac{1}{\lambda_1}\left(\frac{\partial p}{\partial C_1}\right)_1 a=\frac{\cos\mu_1}{\lambda_1}\left[\left(\frac{\partial p}{\partial s}\right)_1-\lambda_1\left(\frac{\partial\delta}{\partial s}\right)_1\right]a \quad \text{(B8)}$$

$$\delta_5=\delta_2+\left(\frac{\partial\delta}{\partial C_1}\right)_2 b=\delta_2-\frac{\sin\mu_2\sin\delta_2}{r}b-\frac{\cos\mu_2}{\lambda_2}\left[\left(\frac{\partial p}{\partial s}\right)_2-\lambda_2\left(\frac{\partial\delta}{\partial s}\right)_2\right]b \quad \text{(B9)}$$

$$\delta_4=\delta_1+\left(\frac{\partial\delta}{\partial C_1}\right)_1 a=\delta_1-\frac{\sin\mu_1\sin\delta_1}{r}a-\frac{\cos\mu_1}{\lambda_1}\left[\left(\frac{\partial p}{\partial s}\right)_1-\lambda_1\left(\frac{\partial\delta}{\partial s}\right)_1\right]a \quad \text{(B10)}$$

When equations (B6) through (B10) are substituted into equation (B5), there is obtained

$$\frac{2\cos\mu_2}{\lambda_2}\left[\left(\frac{\partial p}{\partial s}\right)_2-\lambda_2\left(\frac{\partial\delta}{\partial s}\right)_2\right]b-\frac{2\cos\mu_1}{\lambda_1}\left[\left(\frac{\partial p}{\partial s}\right)_1-\lambda_1\left(\frac{\partial\delta}{\partial s}\right)_1\right]a+$$

$$\frac{\sin\mu_2\sin\delta_2}{r}b-\frac{\sin\mu_1\sin\delta_1}{r}a=\int_4^5\frac{1}{\lambda\cos\mu}\left(\frac{\partial p}{\partial C_1}\right)ds \quad \text{(B11)}$$

If it is assumed that a first approximation to the flow is given by the generalized shock-expansion method, then the right-hand member of equation (B11) may be neglected. Equation (B11) may thus be written

$$\left(\frac{\partial p}{\partial s}\right)_2-\lambda_2\left(\frac{\partial\delta}{\partial s}\right)_2=\frac{\lambda_2}{2r\cos\mu_2}\left[\left(\frac{a}{b}\right)\sin\mu_1\sin\delta_1-\sin\mu_2\sin\delta_2\right]+$$

$$\frac{\cos\mu_1}{\cos\mu_2}\left(\frac{\lambda_2}{\lambda_1}\right)\left(\frac{a}{b}\right)\left[\left(\frac{\partial p}{\partial s}\right)_1-\lambda_1\left(\frac{\partial\delta}{\partial s}\right)_1\right] \quad \text{(B12)}$$

In the limit as the streamline between points 4 and 5 approaches the surface, the ratio, a/b, may be evaluated in terms of the one-dimensional area ratio

$$\frac{a}{b}=\left(\frac{\sin\mu_2}{\sin\mu_1}\right)\frac{\Omega_1}{\Omega_2} \quad \text{(B13)}$$

With the substitution of equation (B13) into (B12), there is obtained after combination of terms

$$\left(\frac{\partial p}{\partial s}\right)_2-\lambda_2\left(\frac{\partial\delta}{\partial s}\right)_2=\frac{B_2}{r}\left(\frac{\Omega_1}{\Omega_2}\sin\delta_1-\sin\delta_2\right)+$$

$$\frac{B_2}{B_1}\frac{\Omega_1}{\Omega_2}\left[\left(\frac{\partial p}{\partial s}\right)_1-\lambda_1\left(\frac{\partial\delta}{\partial s}\right)_1\right] \quad \text{(B14)}$$

where

$$B=\frac{\gamma pM^2}{2(M^2-1)} \quad \text{(B15)}$$

and, of course

$$\lambda=\frac{2\gamma p}{\sin 2\mu} \quad \text{(B16)}$$

$$\Omega=\frac{1}{M}\left[\frac{1+\frac{(\gamma-1)}{2}M^2}{\left(\frac{\gamma+1}{2}\right)}\right]^{\frac{(\gamma+1)}{2(\gamma-1)}} \quad \text{(B17)}$$

Equation (B14) represents only an approximate evaluation of the pressure gradient. More exact evaluations may be found in references 10 and 24. These more exact results, of course, require numerical or graphical integration.

CONCAVE CORNER

In most cases, the tangent bodies used in the application of the present method will have convex corners. There is a possibility that concave corners may be encountered. In the event that the original body does not have sharp concave corners, equation (B14) will still suffice since the flow along the surface is still isentropic. However, if the original body does have sharp concave corners, then the pressure gradient for this case will also be required. This result can be obtained in the same way as equation (B14); however, the shock wave emanating from the corner must be considered after the manner described in reference 9. The expression defining the pressure gradient in this case is

$$\left(\frac{\partial p}{\partial s}\right)_d\left\{\left[\frac{1}{\lambda_d}\left(\frac{\partial p}{\partial\delta}\right)_\sigma\right]\left[\frac{\sin(\sigma-\delta_d)}{\tan\mu_d}\right]+\cos(\sigma-\delta_d)\right\}-\lambda_d\left(\frac{\partial\delta}{\partial s}\right)_d\left\{\left[\frac{\sin(\sigma-\delta_d)}{\tan\mu_d}\right]+\frac{1}{\lambda_d}\left(\frac{\partial p}{\partial\delta}\right)_\sigma\cos(\sigma-\delta_d)\right\}$$

$$=\frac{1}{r}\left(\frac{\partial p}{\partial\delta}\right)_\sigma[\sin(\sigma-\delta_u)\sin\delta_u-\sin(\sigma-\delta_d)\sin\delta_d]+\left(\frac{\partial p}{\partial s}\right)_u\left\{\frac{1}{\lambda_u}\left(\frac{\partial p}{\partial\delta}\right)_\sigma\left[\frac{\sin(\sigma-\delta_u)}{\tan\mu_u}\right]+\left(\frac{p_d}{p_u}-F\right)\cos(\sigma-\delta_u)\right\}-$$

$$\lambda_u\left(\frac{\partial\delta}{\partial s}\right)_u\left\{\left(\frac{p_d}{p_u}-F\right)\left[\frac{\sin(\sigma-\delta_u)}{\tan\mu_u}\right]+\frac{1}{\lambda_u}\left(\frac{\partial p}{\partial\delta}\right)_\sigma\cos(\sigma-\delta_u)\right\}+\frac{F}{\left(1+\frac{\gamma-1}{2}M_u^2\right)^{\frac{\gamma}{\gamma-1}}}\left(\frac{\partial p_t}{\partial n}\right)_u\sin(\sigma-\delta_u) \quad \text{(B18)}$$

where

$$\left(\frac{\partial p}{\partial\delta}\right)_\sigma=\frac{\left(\frac{4\gamma}{\gamma+1}\right)p_uM_u^2\sin(\sigma-\delta_u)\cos(\sigma-\delta_u)}{\left[1-\frac{\sin(\sigma-\delta_d)\cos(\sigma-\delta_d)}{\sin(\sigma-\delta_u)\cos(\sigma-\delta_u)}+\left(\frac{4}{\gamma+1}\right)\frac{\cos^2(\sigma-\delta_d)}{M_u^2\sin^2(\sigma-\delta_u)}\right]} \quad \text{(B19)}$$

and

$$F=\left(\frac{4}{\gamma+1}\right)\left(1+\frac{\gamma-1}{2}M_u^2\right)\sin(\sigma-\delta_u)$$

$$\left\{\frac{[(\gamma+1)\tan(\delta_d-\delta_u)\cos(\sigma-\delta_u)-\sin(\sigma-\delta_u)]M_u^2\sin^2(\sigma-\delta_u)+\sin(\sigma-\delta_u)}{1+[1-2\sin^2(\sigma-\delta_u)+2\tan(\delta_d-\delta_u)\sin(\sigma-\delta_u)\cos(\sigma-\delta_u)]M_u^2\sin^2(\sigma-\delta_u)}\right\} \quad \text{(B20)}$$

In these equations, σ is the shock-wave angle with respect to the body axis, and $(\partial p_t/\partial n)_u$ is the variation of the total pressure normal to the surface just upstream of the shock wave. The subscript, u, refers to conditions upstream of the shock wave, and the subscript, d, refers to conditions downstream. Equation (B18) represents the exact solution

in the usual sense. All effects of the interaction between shock waves and Mach waves are therefore included. In order to be consistent with other parts of this analysis, these effects should be neglected. In addition, since equation (B18) is intended for application to a tangent body, the body curvatures, $(\partial\delta/\partial s)_u$ and $(\partial\delta/\partial s)_d$, will be zero. It

may also be noted that the first step of the tangent body is a cone tangent to the vertex of the original body. For this approximation then, there will be a small layer near the surface of the tangent body for which $(\partial p_l/\partial n)=0$. With these approximations applied to equation (B18), a simplified result can be obtained which will suffice for the present purposes.

$$\left(\frac{\partial p}{\partial s}\right)_d\left[1+\frac{\tan \mu_d}{\tan(\sigma-\delta_d)}\right]=\frac{2B_d}{r}\left[\frac{\sin(\sigma-\delta_u)\sin \delta_u}{\sin(\sigma-\delta_d)}- \sin \delta_d\right]+$$
$$\left(\frac{\partial p}{\partial s}\right)_u\left[\frac{B_d}{B_u}\frac{\sin(\sigma-\delta_u)}{\sin(\sigma-\delta_d)}+\left(\frac{p_d}{p_u}-F\right)\frac{\cos(\sigma-\delta_u)\tan \mu_d}{\sin(\sigma-\delta_d)}\right] \quad (B21)$$

For a body with a concave corner, a special form must also be used for the loading. Just downstream of the corner and before the first convex corner

$$\Lambda=(1-e^{-\eta})\tan \delta\frac{dC_N}{d\alpha}\bigg|_{lcr}+\left(\frac{p_d}{p_u}-F\right)e^{-\eta}\Lambda_u \quad (B22)$$

and, thereafter,

$$\Lambda=(1-e^{-\eta})\tan \delta\frac{dC_N}{d\alpha}\bigg|_{lcr}+\frac{\lambda_2}{\lambda_1}e^{-\eta}\Lambda_1+\left(\frac{p_2}{p_\infty}-\frac{\lambda_2}{\lambda_1}\frac{p_1}{p_\infty}\right)G\Lambda_u \quad (B23)$$

where

$$G=\frac{F}{(p_d/p_\infty)}\left\{\frac{[M_u^2 \sin^2 (\sigma-\delta_u)-1]^2}{[(\gamma-1)M_u^2 \sin^2 (\sigma-\delta_u)+2]M_u^2 \sin^2 (\sigma-\delta_u)}\right\} \quad (B24)$$

The corresponding equations for open-nosed bodies of revolution are similar. The pressure gradient at the leading edge may be determined from equation (B21) with $M_u=M_\infty$, $\delta_u=0$, and $(\partial p/\partial s)_u=0$. The loading on the exterior surface is given by

$$\Lambda=(1-e^{-\eta})\tan \delta\frac{dC_N}{d\alpha}\bigg|_{lcr}+\frac{\lambda_2}{\lambda_1}e^{-\eta}\Lambda_1-\left(\frac{p_2}{p_\infty}-\frac{\lambda_2}{\lambda_1}\frac{p_1}{p_\infty}\right)J\Lambda_v \quad (B25)$$

where Λ_v is the loading at the leading edge, or

$$\Lambda_v=\frac{4 \sin \sigma_v \cos \sigma_v}{(\gamma+1)\left[1-\dfrac{\sin (\sigma_v-\delta_v) \cos (\sigma_v-\delta_v)}{\sin \sigma_v \cos \sigma_v}+\left(\dfrac{4}{\gamma+1}\right)\dfrac{\cos^2 (\sigma_v-\delta_v)}{M_\infty^2 \sin^2 \sigma_v}\right]} \quad (B26)$$

and J is defined by

$$J=\frac{(M_\infty^2 \sin^2 \sigma_v-1)^2}{(p_v/p_\infty)M_\infty^3 \sin^3 \sigma_v[(\gamma-1)M_\infty^2 \sin^2 \sigma_v+2]} \quad (B27)$$

For bodies with concave corners, and for open-nosed

bodies, the total pressure is not constant on the surface when the bodies are inclined. This variation in surface total pressure leads to the term involving Λ_u in equation (B23) and the term involving Λ_v in equation (B25).

APPENDIX C

EXTENSIONS OF THE APPROXIMATE METHOD

This analysis is based on the approximate or two-step method previously mentioned. The basic equations of this method are equations (11), (12), (13), and (20). Before proceeding with this analysis, it is convenient to write down the expressions for the function β (see eq. (12)) for several types of bodies. These expressions are presented in the following table:

EXPRESSIONS FOR β

Body	For nose section	For cylindrical afterbody
Any body	$\dfrac{x \sin \delta_v-r \cos \delta_v}{r \cos \delta-x \sin \delta}$	$2f_n \sin \delta_v\left(\dfrac{x}{l_n}\right)-\cos \delta_v$
Cone-cylinder	(Not required)	$\dfrac{2f_n\left(\frac{x}{l_n}-1\right)}{\sqrt{1+4f_n^2}}$
Tangent-ogive-cylinder	1	$\dfrac{1+4f_n^2\left(2\frac{x}{l_n}-1\right)}{1+4f_n^2}$
Tangent-paraboloid cylinder	$\sqrt{\dfrac{f_n^2+\left(1-\frac{x}{l_n}\right)^2}{_n^2+1}}$	$\dfrac{f_n\left(2\frac{x}{l_n}-1\right)}{\sqrt{f_n^2+1}}$

In general, the equations for the normal-force and pitching-moment derivatives may be integrated in two parts—one part for the nose section and one for the afterbody. Thus, with the loading defined by equation (20)

$$\frac{dC_N}{d\alpha}=\frac{dC_N}{d\alpha}\bigg|_{nose}+G_1e^{-G_2f_n}(1-e^{-G_2f_a}) \quad (C1)$$

$$\frac{dC_m}{d\alpha}=\frac{dC_m}{d\alpha}\bigg|_{nose}-\frac{G_1}{G_2}e^{-G_2f_n}[(1+G_2f_n)-(1+G_2f_n+G_2f_a)e^{-G_2f_a}] \quad (C2)$$

where

$$G_1=\frac{2}{\psi_a\cos \delta_v}\frac{p_{s_a}}{p_v}\frac{\sin 2\mu_v}{\sin 2\mu_{s_a}}\frac{dC_N}{d\alpha}\bigg|_{lcr}e^{\psi_a\cos \delta_v} \quad (C3)$$

and

$$G_2=2\psi_a\sin \delta_v \quad (C4)$$

The additional subscript, a, refers to functions evaluated for the afterbody (i. e., $\delta=0$). Thus, from equation (13),

$$\psi_a=\frac{\gamma(p_{s_a}/p_\infty)M_{s_a}^2}{2(1-p_{s_a}/p_\infty)(M_{s_a}^2-1)}\frac{\Omega_v}{\Omega_{s_a}} \quad (C5)$$

The terms G_1 and G_2 are functions of M_∞ and δ_v alone. These functions have been evaluated and the results are shown in figure 12.

(a) Function, G_1
(b) Function, G_2
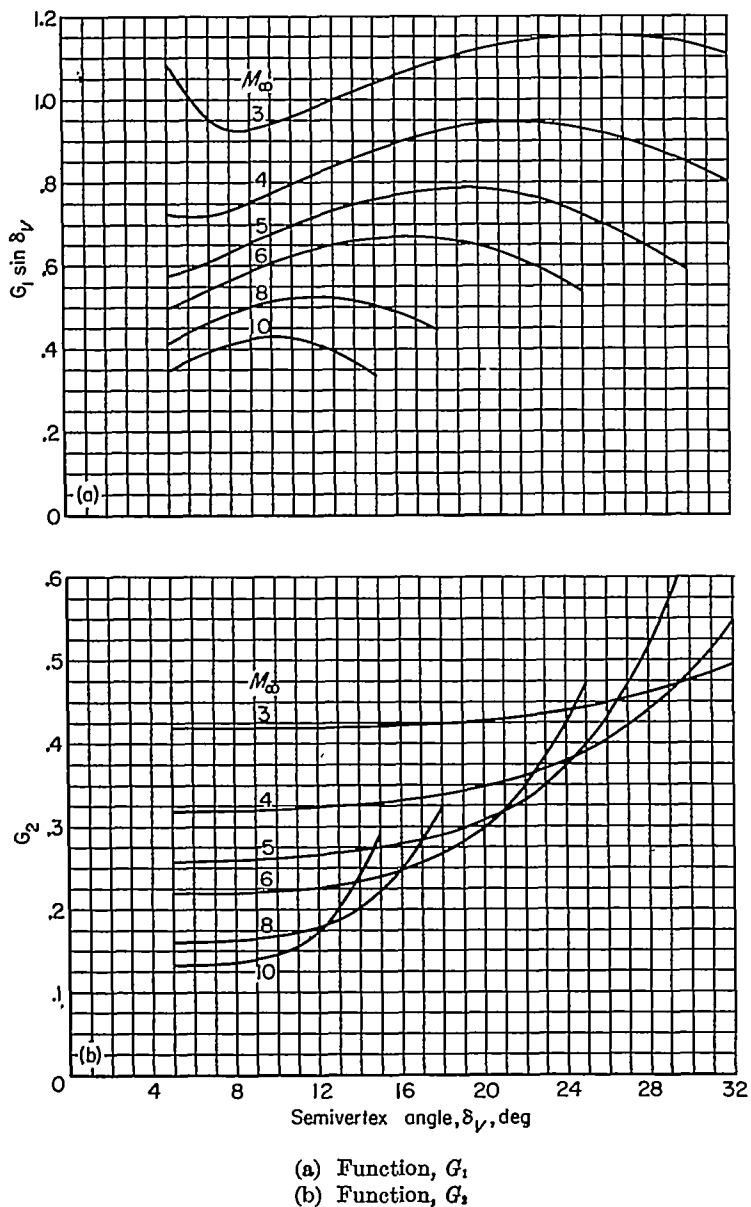
FIGURE 12.—Curves defining functions G_1 and G_2 (Appendix C).

For the special case of cone-cylinders, equations (C1) and (C2) represent a closed solution of the general method as well.

By the use of an additional approximation to Λ, results in closed form can also be obtained for ogival nose sections. Such an approximation is

$$\Lambda = G_3 \tan \delta_v \left(\frac{dC_N}{d\alpha}\right)_{tc_v} + G_4 \tan \delta + \frac{\left[(1-G_3)\frac{dC_N}{d\alpha}\Big|_{tc_v} - G_4\right](\tan \delta)^2}{\tan \delta_v}$$

$$(C6)$$

where

$$G_3 = \frac{p_{s_a}}{p_v} \frac{\sin 2\mu_v}{\sin 2\mu_{s_a}} e^{-\psi_a} \qquad (C7)$$

and

$$G_4 = 2(1 - e^{-\psi_a}) \qquad (C8)$$

When equation (C6) is substituted in equations (14) and (21), equations are obtained in closed form for $dC_N/d\alpha$ and $dC_m/d\alpha$. These equations involve constants which are complicated functions of the nose angle δ_v (or nose fineness ratio f_x). These functions can be expanded in a series in terms of δ_t; the leading terms of these series are constants independent of δ_v. In view of the approximate nature of this analysis, the use of the leading terms will suffice. Thus there is obtained

$$\frac{dC_N}{d\alpha}\bigg|_{ogive} = \frac{7}{15} G_4 + \frac{8}{15}(1+4G_3)\left(\frac{dC_N}{d\alpha}\right)_{tc_v} \qquad (C9)$$

$$\frac{1}{f_x}\frac{dC_m}{d\alpha}\bigg|_{ogive} = -\frac{4}{15} G_4 - \frac{(3+22G_3)}{15}\left(\frac{dC_N}{d\alpha}\right)_{tc_v} \qquad (C10)$$

To the accuracy of this analysis, these equations also represent the solutions for a tangent paraboloid. These equations have been evaluated for a range of Mach numbers and nose fineness ratios. The results are presented in figure 13. It is apparent that with the aid of equations (C1), (C2), (C9), (C10), and figures 12 and 13, $dC_N/d\alpha$ and $dC_m/d\alpha$ for ogive-cylinders can be evaluated approximately in a few minutes.
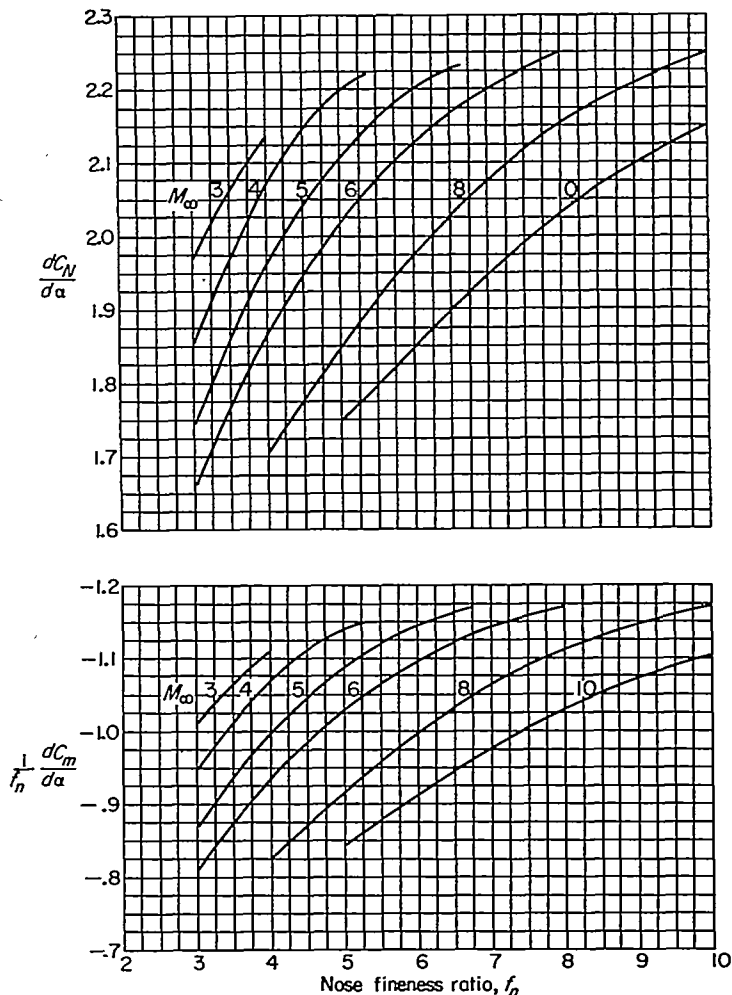
FIGURE 13.—Curves defining normal-force and pitching-moment derivatives for tangent ogives as predicted by approximate closed solution of Appendix C.

REFERENCES

1. Eggers, A. J., Jr., and Savin, Raymond C.: A Unified Two-Dimensional Approach to the Calculation of Three-Dimensional Hypersonic Flows, With Application to Bodies of Revolution. NACA Rep. 1249, 1955. (Supersedes NACA TN 2811.)
2. Eggers, A. J., Jr., and Savin, Raymond C.: Approximate Methods for Calculating the Flow About Nonlifting Bodies of Revolution at High Supersonic Airspeeds. NACA TN 2579, 1951.
3. Savin, Raymond C.: Application of the Generalized Shock-Expansion Method to Inclined Bodies of Revolution Traveling at High Supersonic Airspeeds. NACA TN 3349, 1955.
4. Eggers, A. J., Jr., Savin, Raymond C., and Syvertson, Clarence A.: The Generalized Shock-Expansion Method and Its Application to Bodies Traveling at High Supersonic Airspeeds. Jour. Aero. Sci., vol. 22, no. 4, Apr. 1955, pp. 231–238.
5. Van Dyke, Milton D.: A Study of Second-Order Supersonic Flow Theory. NACA Rep. 1081, 1952. (Supersedes NACA TN 2200.)
6. Van Dyke, Milton D.: First- and Second-Order Theory of Supersonic Flow Past Bodies of Revolution. Jour. Aero. Sci., vol. 18, no. 3, Mar. 1951, pp. 161–179.
7. Van Dyke, Milton D.: A Study of Hypersonic Small-Disturbance Theory. NACA TN 3173, 1954.
8. Van Dyke, Milton D.: Applications of Hypersonic Small-Disturbance Theory. Jour. Aero. Sci., vol. 21, no. 3, Mar. 1954, pp. 179–186.
9. Eggers, A. J., Jr., Syvertson, Clarence A., and Kraus, Samuel: A Study of Inviscid Flow About Airfoils at High Supersonic Speeds. NACA Rep. 1123, 1953. (Formerly NACA TN's 2646 and 2729.)
10. Ferrari, C.: The Supersonic Flow About a Sharp Nosed Body of Revolution. Brown University, Providence, R. I., Graduate Division of Applied Mathematics, Translation A9–T–18, 1948. (Translated from: Campo Aerodinamico a Velocita Iperacustica Attorno a un Solido di Rivoluzione a Prora Acuminata. L'Aerotecnica, vol. XVI, no. 2, pp. 121–130, 1936.)
11. Ehret, Dorris M., Rossow, Vernon J., and Stevens, Victor I.: An Analysis of the Applicability of the Hypersonic Similarity Law to the Study of Flow About Bodies of Revolution at Zero Angle of Attack. NACA TN 2250, 1950.
12. Staff of the Computing Section, Center of Analysis (Under Direction of Zdenek Kopal): Tables of Supersonic Flow Around Cones. Tech. Rep. No. 1, M. I. T., Dept. of Elect. Engr., Cambridge, 1947.
13. Ferri, Antonio: Supersonic Flow Around Circular Cones at Angles of Attack. NACA Rep. 1045, 1951. (Supersedes NACA TN 2236.)
14. Staff of the Computing Section, Center of Analysis (Under Direction of Zdenek Kopal): Tables of Supersonic Flow Around Yawing Cones. Tech. Rep. No. 3, M. I. T., Dept. of Elect. Engr., Cambridge, 1947.
15. Dorrance, W. H.: Theoretical Center of Pressure and First Order Theory for Bodies of Revolution. Convair Corp., A-Atlas-30, 1952.
16. Eggers, A. J., Jr., and Nothwang, George J.: The Ames 10- by 14-Inch Supersonic Wind Tunnel. NACA TN 3095, 1954.
17. Rossow, Vernon J.: Applicability of the Hypersonic Similarity Rule to Pressure Distributions Which Include the Effects of Rotation for Bodies of Revolution at Zero Angle of Attack. NACA TN 2399, 1951.
18. Ehret, Dorris M.: Accuracy of Approximate Methods for Predicting Pressures on Pointed Nonlifting Bodies of Revolution in Supersonic Flow. NACA TN 2764, 1952.
19. Tsien, Hsue-Shen: Supersonic Flow Over an Inclined Body of Revolution. Jour. Aero. Sci., vol. 5, no. 12, Oct. 1938, pp. 480–483.
20. Grimminger, G., Williams, E. P., and Young, G. B. W.: Lift on Inclined Bodies of Revolution in Hypersonic Flow. Jour. Aero. Sci., vol. 17, no. 11, Nov. 1950, pp. 675–690.
21. Van Dyke, Milton D.: Practical Calculation of Second-Order Supersonic Flow Past Nonlifting Bodies of Revolution. NACA TN 2744, 1952.
22. Huth, J. H., and Dye, H.: Axial and Normal Force Coefficients for Pointed Bodies of Revolution at Super- and Hypersonic Speeds. Part I. Noses and Cylinders. RAND Res. Memo., RM–844, May 21, 1952.
23. McCauley, William D., and Feller, William V.: An Investigation of the Characteristics of the NACA RM–10 (With and Without Fins) in the Langley 11-Inch Hypersonic Tunnel at a Mach Number of 6.9. NACA RM L54I03, 1954.
24. Johannsen, N. H., and Meyer, R. E.: Axially-Symmetrical Supersonic Flow Near the Center of an Expansion. Aero. Quart., vol. II, Aug. 1950, pp. 127–142.

TABLE I.—NORMAL-FORCE DERIVATIVES AT ZERO ANGLE OF ATTACK

Nose shape	M_∞	f_a	First-order potential theory	Van Dyke hybrid potential theory	Second-order shock-expansion method	Generalized shock-expansion method	Newtonian impact theory	Experiment
Cone, $f_n=7$	3.00	0	1.97	1.98	1.91	1.91	1.99	1.97
	--	2	2.49	2.49	2.47	2.75	------	2.52
	--	4	2.50	2.50	2.70	3.59	------	2.69
	--	6	2.38	2.39	2.80	4.43	------	2.78
	--	8	2.30	2.29	2.84	5.28	------	------
	--	10	2.25	2.25	2.86	6.12	------	2.84
	4.24	0	1.94	1.96	1.89	1.89	1.99	1.83
	--	2	2.53	2.54	2.44	2.64	------	2.38
	--	4	2.74	2.74	2.73	3.39	------	2.68
	--	6	2.71	2.72	2.88	4.14	------	2.86
	--	8	2.62	2.62	2.96	4.88	------	------
	--	10	2.53	2.53	3.00	5.64	------	2.85
	5.05	0	1.92	1.95	1.88	1.88	1.99	1.91
	--	2	2.53	2.54	2.41	2.58	------	2.35
	--	4	2.81	2.82	2.72	3.33	------	2.65
	--	6	2.88	2.89	2.89	3.95	------	2.86
	--	8	2.84	2.84	2.99	4.67	------	------
	--	10	2.75	2.76	3.05	5.35	------	3.06
	6.28	0	1.88	1.94	1.88	1.88	1.99	1.92
	--	2	2.49	2.53	2.38	2.51	------	2.31
	--	4	2.86	2.88	2.69	3.14	------	2.58
	--	6	3.03	3.06	2.89	3.78	------	2.81
	--	8	3.07	3.10	3.00	4.41	------	------
	--	10	3.04	3.07	3.08	5.04	------	2.99
Cone, $f_n=5$	3.00	0	1.95	1.96	1.88	1.88	1.98	1.83
	--	2	2.65	2.66	2.59	2.93	------	2.60
	--	4	2.71	2.73	2.89	3.98	------	2.89
	--	6	2.58	2.59	3.02	5.02	------	2.90
	--	8	2.46	2.48	3.08	6.08	------	------
	--	10	2.41	2.42	3.10	7.12	------	3.01
	4.24	0	1.90	1.95	1.87	1.87	1.98	1.82
	--	2	2.68	2.70	2.54	2.77	------	2.46
	--	4	2.98	2.99	2.91	3.68	------	2.84
	--	6	3.00	3.02	3.11	4.58	------	3.01
	--	8	2.92	2.93	3.22	5.49	------	------
	--	10	2.81	2.82	3.27	6.39	------	3.21
	5.05	0	1.86	1.95	1.87	1.87	1.98	1.91
	--	2	2.66	2.70	2.51	2.69	------	2.48
	--	4	3.06	3.09	2.90	3.52	------	2.80
	--	6	3.18	3.21	3.13	4.34	------	3.21
	--	8	3.16	3.19	3.27	5.16	------	------
	--	10	3.07	3.10	3.35	5.99	------	3.26
	6.28	0	1.80	1.96	1.88	1.88	1.98	1.83
	--	2	2.59	2.69	2.46	2.60	------	2.49
	--	4	3.09	3.16	2.84	3.32	------	2.72
	--	6	3.34	3.40	3.08	4.04	------	2.98
	--	8	3.44	3.50	3.24	4.77	------	------
	--	10	3.43	3.50	3.33	5.49	------	3.22
Cone, $f_n=3$	3.00	0	1.88	1.95	1.83	1.83	1.95	1.86
	--	2	2.97	2.99	2.74	3.18	------	2.72
	--	4	3.16	3.18	3.13	4.54	------	3.15
	--	6	3.03	3.05	3.29	5.89	------	3.25
	--	8	2.90	2.91	3.36	7.25	------	------
	--	10	2.82	2.84	3.40	8.60	------	3.37
	4.24	0	1.78	1.99	1.85	1.85	1.95	1.83
	--	2	2.93	3.04	2.66	2.94	------	2.55
	--	4	3.45	3.53	3.10	4.04	------	3.12
	--	6	3.57	3.65	3.33	5.14	------	3.28
	--	8	3.51	3.58	3.45	6.23	------	------
	--	10	3.40	3.47	3.52	7.33	------	3.45
	5.05	0	1.71	2.05	1.86	1.86	1.95	1.88
	--	2	2.86	3.06	2.61	2.82	------	2.55
	--	4	3.50	3.65	3.05	3.78	------	3.12
	--	6	3.72	3.91	3.31	4.74	------	3.44
	--	8	3.82	3.96	3.46	5.70	------	------
	--	10	3.76	3.90	3.55	6.66	------	3.63
	6.28	0	------	------	1.88	1.88	1.95	1.88
	--	2	------	------	2.53	2.67	------	2.58
	--	4	------	------	2.95	3.46	------	2.87
	--	6	------	------	3.22	4.25	------	3.19
	--	8	------	------	3.40	5.04	------	------
	--	10	------	------	3.52	5.83	------	3.37

Nose shape	M_∞	f_a	First-order potential theory	Van Dyke hybrid potential theory	Second-order shock-expansion method			Generalized shock-expansion method	Newtonian impact theory	Experiment
					Ten-step solution	Two-step approximation	Appendix C			
Ogive, $f_n=7$	3.00	0	2.53	2.53	2.39	2.16	2.23	3.67	1.97	2.51
	--	2	2.65	2.65	2.72	2.35	2.42	4.94	----	2.72
	--	4	2.57	2.57	2.86	2.43	2.50	6.22	----	2.84
	--	6	2.46	2.46	2.91	2.46	2.53	7.49	----	2.84
	--	8	2.42	2.42	2.94	2.48	2.54	8.76	----	----
	--	10	2.40	2.40	2.94	2.48	2.55	10.03	----	2.85
	4.24	0	2.64	2.64	2.40	2.20	2.25	3.29	1.97	2.40
	--	2	2.96	2.97	2.77	2.45	2.51	4.34	----	2.64
	--	4	3.02	3.02	2.95	2.58	2.64	5.39	----	2.92
	--	6	2.95	2.95	3.04	2.65	2.71	6.44	----	3.11
	--	8	2.86	2.87	3.09	2.69	2.75	7.49	----	----
	--	10	2.79	2.80	3.11	2.71	2.77	8.54	----	3.11
	5.05	0	2.67	2.71	2.38	2.23	2.24	3.08	1.97	2.29
	--	2	3.06	3.07	2.77	2.52	2.53	4.01	----	2.68
	--	4	3.19	3.20	2.99	2.69	2.70	4.94	----	2.86
	--	6	3.18	3.19	3.11	2.79	2.81	5.87	----	2.94
	--	8	3.11	3.12	3.17	2.85	2.87	6.80	----	----
	--	10	3.02	3.02	3.21	2.88	2.90	7.73	----	3.02
	6.28	0	2.65	2.65	2.35	2.24	2.18	2.81	1.97	2.23
	--	2	3.13	3.10	2.73	2.54	2.48	3.59	----	2.53
	--	4	3.41	3.34	2.95	2.73	2.67	4.37	----	2.83
	--	6	3.50	3.43	3.09	2.86	2.80	5.15	----	2.96
	--	8	3.49	3.43	3.17	2.94	2.88	5.93	----	----
	--	10	3.43	3.38	3.21	2.99	2.93	6.71	----	3.24
Ogive, $f_n=5$	3.00	0	2.66	2.65	2.35	2.15	2.22	3.22	1.95	2.47
	--	2	2.98	2.97	2.84	2.48	2.55	4.68	----	2.75
	--	4	2.92	2.91	3.06	2.61	2.68	6.13	----	2.95
	--	6	2.80	2.79	3.15	2.67	2.74	7.58	----	3.01
	--	8	2.72	2.71	3.19	2.69	2.76	9.03	----	----
	--	10	2.69	2.68	3.20	2.70	2.77	10.48	----	3.06
	4.24	0	2.69	2.69	2.30	2.16	2.16	2.84	1.95	2.35
	--	2	3.28	3.23	2.80	2.54	2.54	3.98	----	2.76
	--	4	3.44	3.38	3.06	2.74	2.74	5.12	----	2.96
	--	6	3.41	3.36	3.19	2.84	2.84	6.25	----	3.01
	--	8	3.32	3.26	3.25	2.90	2.90	7.38	----	----
	--	10	3.22	3.16	3.28	2.93	2.92	8.52	----	3.18
	5.05	0	----	----	2.27	2.15	2.10	2.63	1.95	2.18
	--	2	----	----	2.77	2.53	2.48	3.61	----	2.66
	--	4	----	----	3.04	2.76	2.71	4.58	----	2.93
	--	6	----	----	3.19	2.89	2.84	5.56	----	3.24
	--	8	----	----	3.28	2.96	2.91	6.54	----	----
	--	10	----	----	3.33	3.01	2.96	7.51	----	3.29
	6.28	0	----	----	2.23	2.11	1.99	2.37	1.95	2.12
	—	2	----	----	2.70	2.47	2.36	3.16	----	2.57
	--	4	----	----	2.97	2.71	2.59	3.94	----	2.78
	--	6	----	----	3.13	2.86	2.74	4.73	----	3.01
	--	8	----	----	3.23	2.95	2.83	5.52	----	----
	--	10	----	----	3.28	3.01	2.89	6.30	----	3.31
Ogive, $f_n=3$	3.00	0	----	----	2.19	2.06	1.99	2.50	1.86	2.28
	—	2	----	----	2.87	2.60	2.53	4.06	----	2.93
	--	4	----	----	3.13	2.82	2.75	5.63	----	3.25
	--	6	----	----	3.23	2.92	2.84	7.19	----	3.20
	--	8	----	----	3.27	2.96	2.88	8.76	----	----
	--	10	----	----	3.28	2.97	2.90	10.32	----	3.32
	4.24	0	----	----	2.10	1.98	1.83	2.16	1.86	2.09
	--	2	----	----	2.76	2.46	2.31	3.28	----	2.81
	--	4	----	----	3.06	2.70	2.56	4.40	----	3.11
	--	6	----	----	3.24	2.83	2.68	5.53	----	3.29
	--	8	----	----	3.32	2.89	2.74	6.65	----	----
	--	10	----	----	3.36	2.93	2.78	7.77	----	3.34
	5.05	0	----	----	1.98	1.88	1.74	1.97	1.86	2.01
	--	2	----	----	2.59	2.32	2.17	2.90	----	2.66
	--	4	----	----	2.90	2.55	2.41	3.82	----	2.93
	--	6	----	----	3.05	2.68	2.53	4.74	----	3.16
	--	8	----	----	3.13	2.75	2.60	5.67	----	----
	--	10	----	----	3.17	2.79	2.64	6.59	----	3.38
	6.28	0	----	----	1.79	1.72	1.65	1.77	1.86	1.83
	--	2	----	----	2.32	2.06	1.99	2.50	----	2.44
	--	4	----	----	2.53	2.26	2.18	3.22	----	2.61
	--	6	----	----	2.70	2.36	2.29	3.94	----	2.67
	--	8	----	----	2.77	2.42	2.35	4.67	----	----
	--	10	----	----	2.80	2.45	2.38	5.39	----	2.90

TABLE II.—CENTERS OF PRESSURE AT ZERO ANGLE OF ATTACK

Nose shape	M_∞	f_a	First-order potential theory	Van Dyke hybrid potential theory	Second-order shock-expansion method	Generalized shock-expansion method	Newtonian impact theory	Experiment
Cone, f_a=7	3.00	0	4.67	4.67	4.67	4.67	4.67	4.75
--	--	2	5.32	5.34	5.39	5.69	------	5.56
--	--	4	5.34	5.32	5.78	6.70	------	5.63
--	--	6	5.00	5.00	5.99	7.70	------	5.85
--	--	8	4.63	4.63	6.11	8.71	------	------
--	--	10	4.42	4.41	6.17	9.72	------	6.32
--	4.24	0	4.67	4.67	4.67	4.67	4.67	4.61
--	--	2	5.41	5.41	5.40	5.61	------	5.55
--	--	4	5.72	5.72	5.88	6.59	------	6.00
--	--	6	5.69	5.68	8.20	7.57	------	6.40
--	--	8	5.33	5.38	6.40	8.55	------	------
--	--	10	5.00	5.00	6.53	9.55	------	6.39
--	5.05	0	4.67	4.67	4.67	4.67	4.67	4.71
--	--	2	5.46	5.44	5.39	5.57	------	5.45
--	--	4	5.92	5.89	5.89	6.40	------	5.86
--	--	6	6.04	6.00	6.25	7.53	------	6.28
--	--	8	5.91	5.87	6.51	8.45	------	------
--	--	10	5.62	5.58	6.69	9.48	------	6.55
--	6.28	0	4.67	4.67	4.67	4.67	4.67	4.74
--	--	2	5.46	5.42	5.35	5.50	------	5.40
--	--	4	6.04	5.98	5.88	6.41	------	5.80
--	--	6	6.38	6.30	6.29	7.35	------	6.31
--	--	8	6.48	6.40	6.59	8.30	------	------
--	--	10	6.40	6.32	6.81	9.27	------	6.74
Cone, f_a=5	3.00	0	3.33	3.33	3.33	3.33	3.33	3.35
--	--	2	4.02	3.98	4.02	4.29	------	4.04
--	--	4	4.09	4.05	4.43	5.27	------	4.46
--	--	6	3.78	3.75	4.66	6.26	------	4.53
--	--	8	3.41	3.37	4.79	7.25	------	------
--	--	10	3.16	3.13	4.86	8.24	------	4.88
--	4.24	0	3.33	3.33	3.33	3.33	3.33	3.26
--	--	2	4.07	4.05	4.01	4.21	------	4.02
--	--	4	4.46	4.41	4.50	5.14	------	4.47
--	--	6	4.45	4.41	4.85	6.10	------	4.98
--	--	8	4.20	4.16	5.08	7.07	------	------
--	--	10	3.84	3.81	5.24	8.06	------	5.39
--	5.05	0	3.33	3.33	3.33	3.33	3.33	3.38
--	--	2	4.10	4.04	4.00	4.15	------	3.99
--	--	4	4.59	4.52	4.52	5.06	------	4.54
--	--	6	4.80	4.72	4.92	6.00	------	5.08
--	--	8	4.74	4.65	5.21	6.95	------	------
--	--	10	4.48	4.42	5.43	7.92	------	5.25
--	6.28	0	3.33	3.33	3.33	3.33	3.33	3.25
--	--	2	4.13	4.04	3.95	4.07	------	4.12
--	--	4	4.72	4.60	4.48	4.93	------	4.48
--	--	6	5.14	5.00	4.91	5.83	------	4.95
--	--	8	5.31	5.16	5.25	6.77	------	------
--	--	10	5.29	5.14	5.52	7.73	------	5.32
Cone, f_a=3	3.00	0	2.00	2.00	2.00	2.00	2.00	2.08
--	--	2	2.67	2.63	2.62	2.85	------	2.70
--	--	4	2.85	2.80	3.02	3.79	------	3.10
--	--	6	2.61	2.57	3.27	4.76	------	3.10
--	--	8	2.25	2.20	3.40	5.74	------	------
--	--	10	2.00	1.96	3.48	6.72	------	3.51
--	4.24	0	2.00	2.00	2.00	2.00	2.00	2.19
--	--	2	2.74	2.65	2.58	2.75	------	2.68
--	--	4	3.20	3.08	3.05	3.63	------	3.18
--	--	6	3.34	3.26	3.38	4.56	------	3.35
--	--	8	3.33	3.12	3.61	5.52	------	------
--	--	10	2.94	2.84	3.77	6.49	------	3.82
--	5.05	0	2.00	2.00	2.00	2.00	2.00	2.10
--	--	2	2.77	2.65	2.55	2.63	------	2.52
--	--	4	3.35	3.19	3.02	3.52	------	3.23
--	--	6	3.67	3.50	3.42	4.43	------	3.37
--	--	8	3.74	3.56	3.71	5.37	------	------
--	--	10	3.59	3.43	3.92	6.33	------	3.82
--	6.28	0	------	------	2.00	2.00	2.00	2.03
--	--	2	------	------	2.49	2.59	------	2.52
--	--	4	------	------	2.98	3.37	------	3.16
--	--	6	------	------	3.40	4.23	------	3.50
--	--	8	------	------	3.75	5.13	------	------
--	--	10	------	------	3.98	6.07	------	3.77

Nose shape	M_∞	f_a	First-order potential theory	Van Dyke hybrid potential theory	Second-order shock-expansion method			Generalized shock-expansion method	Newtonian impact theory	Experiment
					Ten-step solution	Two-step approximation	Appendix C			
Ogive, f_a=7	3.00	0	3.69	3.66	3.73	3.59	3.58	4.17	3.17	3.79
--	--	2	3.85	3.82	4.23	3.93	3.91	5.16	----	4.12
--	--	4	3.62	3.59	4.50	4.12	4.10	6.15	----	4.32
--	--	6	3.29	3.26	4.63	4.23	4.21	7.14	----	4.40
--	--	8	3.04	3.00	4.70	4.28	4.26	8.14	----	----
--	--	10	2.97	2.93	4.74	4.31	4.29	9.14	----	4.55
--	4.24	0	3.80	3.76	3.75	3.66	3.63	4.11	3.17	3.70
--	--	2	4.26	4.21	4.30	4.10	4.06	5.05	----	4.08
--	--	4	4.34	4.29	4.65	4.40	4.35	6.02	----	4.76
--	--	6	4.20	4.15	4.87	4.60	4.55	6.99	----	4.08
--	--	8	3.86	3.80	5.00	4.73	4.68	7.97	----	----
--	--	10	3.53	3.48	5.08	4.81	4.76	8.96	----	5.16
--	5.05	0	3.85	3.77	3.75	3.66	3.64	4.04	3.17	3.75
--	--	2	4.40	4.31	4.34	4.15	4.13	4.96	----	4.32
--	--	4	4.61	4.53	4.73	4.52	4.50	5.91	----	4.86
--	--	6	4.57	4.48	5.01	4.79	4.76	6.87	----	5.10
--	--	8	4.34	4.26	5.19	4.98	4.96	7.85	----	----
--	--	10	4.04	3.95	5.31	5.12	5.09	8.83	----	5.23
--	6.28	0	3.88	3.74	3.72	3.64	3.62	3.97	3.17	3.65
--	--	2	4.50	4.37	4.31	4.14	4.14	4.85	----	4.20
--	--	4	4.86	4.74	4.74	4.55	4.55	5.77	----	4.70
--	--	6	5.05	4.94	5.05	4.88	4.89	6.71	----	5.10
--	--	8	5.03	4.92	5.27	5.13	5.15	7.67	----	----
--	--	10	4.88	4.74	5.42	5.32	5.34	8.64	----	5.58
Ogive, f_a=5	3.00	0	2.69	2.68	2.68	2.60	2.60	2.91	2.30	2.70
--	--	2	3.00	3.00	3.22	3.03	3.01	3.87	----	3.02
--	--	4	2.88	2.88	3.55	3.28	3.26	4.85	----	3.35
--	--	6	2.56	2.56	3.73	3.42	3.39	5.84	----	3.50
--	--	8	2.30	2.29	3.83	3.49	3.46	6.82	----	----
--	--	10	2.16	2.15	3.88	3.53	3.50	7.82	----	3.75
--	4.24	0	2.74	2.66	2.66	2.59	2.59	2.84	2.30	2.70
--	--	2	3.28	3.21	3.24	3.08	3.08	3.74	----	3.15
--	--	4	3.48	3.43	3.62	3.42	3.43	4.63	----	3.50
--	--	6	3.39	3.34	3.87	3.66	3.67	5.65	----	3.75
--	--	8	3.12	3.06	4.03	3.82	3.82	6.63	----	----
--	--	10	2.76	2.70	4.13	3.92	3.92	7.61	----	4.09
--	5.05	0	----	----	2.64	2.58	2.57	2.79	2.30	2.70
--	--	2	----	----	3.23	3.08	3.09	3.66	----	3.20
--	--	4	----	----	3.65	3.48	3.49	4.58	----	3.73
--	--	6	----	----	3.94	3.77	3.78	5.53	----	3.85
--	--	8	----	----	4.15	3.98	3.99	6.50	----	----
--	--	10	----	----	4.28	4.12	4.14	7.47	----	4.06
--	6.28	0	----	----	2.62	2.55	2.54	2.72	2.30	2.02
--	--	2	----	----	3.19	3.05	3.06	3.54	----	3.13
--	--	4	----	----	3.62	3.47	3.49	4.43	----	3.60
--	--	6	----	----	3.94	3.80	3.85	5.38	----	4.00
--	--	8	----	----	4.20	4.06	4.12	6.30	----	----
--	--	10	----	----	4.34	4.26	4.33	7.26	----	4.32
Ogive, f_a=3	3.00	0	----	----	1.59	1.56	1.56	1.70	1.35	1.65
--	--	2	----	----	2.12	2.03	2.04	2.59	----	2.12
--	--	4	----	----	2.43	2.34	2.35	3.53	----	2.45
--	--	6	----	----	2.60	2.52	2.54	4.51	----	2.49
--	--	8	----	----	2.68	2.62	2.64	5.49	----	----
--	--	10	----	----	2.73	2.67	2.69	6.47	----	2.60
--	4.24	0	----	----	1.56	1.52	1.52	1.61	1.35	1.58
--	--	2	----	----	2.11	1.98	2.01	2.43	----	2.17
--	--	4	----	----	2.51	2.34	2.38	3.34	----	2.44
--	--	6	----	----	2.76	2.53	2.64	4.28	----	2.75
--	--	8	----	----	2.93	2.74	2.80	5.24	----	----
--	--	10	----	----	3.03	2.84	2.91	6.22	----	3.12
--	5.05	0	----	----	1.55	1.51	1.48	1.58	1.35	1.47
--	--	2	----	----	2.26	1.96	1.97	2.35	----	2.25
--	--	4	----	----	2.79	2.32	2.35	3.23	----	2.75
--	--	6	----	----	3.19	2.59	2.63	4.16	----	3.15
--	--	8	----	----	3.49	2.77	2.83	5.11	----	----
--	--	10	----	----	3.73	2.90	2.96	6.08	----	3.60
--	6.28	0	----	----	1.52	1.50	1.45	1.53	1.35	1.53
--	--	2	----	----	2.06	1.90	1.88	2.25	----	2.10
--	--	4	----	----	2.45	2.24	2.23	3.09	----	2.45
--	--	6	----	----	2.71	2.49	2.49	3.99	----	2.60
--	--	8	----	----	2.87	2.67	2.67	4.92	----	----
--	--	10	----	----	2.98	2.79	2.80	5.87	----	3.05